Catal Lett (2015) 145:483–504
DOI 10.1007/s10562-014-1343-0

PERSPECTIVE

# Storage and Reduction of $NO_x$ Over LNT Catalysts

**P. Forzatti · L. Lietti · L. Castoldi**

Received: 21 August 2014 / Accepted: 21 August 2014 / Published online: 11 September 2014


**Abstract** In this paper, fundamental issues of the NSR technology are addressed. The reaction paths and the mechanism involved in the storage of $NO_x$ and the relevance of the proximity between the noble metal and the alkali or alkaline-earth component of the catalyst are discussed first. Then the release of $NO_x$, the reaction pathways of $NO_x$ reduction by different reducing agents, and the mechanisms involved in the formation of $N_2$, $NH_3$ and $N_2O$ are illustrated. The use of the combined technologies LNT + SCR and DPNR is addressed next and key aspects that highlight the synergies of the individual technologies are discussed. Finally, the perspectives of the NSR technology are outlined.

**Keywords** $NO_x$ storage reduction catalysts · Lean $NO_x$ trap · Pt–Ba catalysts · $N_2O$ formation · Isotopic exchange experiments · $NO_x$ reduction under lean conditions

## 1 Introduction

Environmental policy in industrialized countries forces a drastic reduction of $NO_x$ emissions from diesel engines that operate under lean conditions and have significantly better fuel economy compared to gasoline stoichiometric engines. The EU emission standards for passenger cars are summarized in Table 1 [1]. Since the Euro 2 stage, EU regulations introduce different emission limits for diesel and gasoline vehicles. Diesel have more stringent CO standards but are allowed higher $NO_x$. However, significant reductions in $NO_x$ limits are introduced for diesel engines with Euro 6 (from 0.18 g/km in Euro 5 down to 0.08 g/km in Euro 6), which makes $NO_x$ emission standards essentially fuel neutral (0.08 g/km in diesel engines vs. 0.06 g/km in gasoline engines). Table 1 also shows that gasoline vehicles are exempted from particulate matter (PM) standards through the Euro 4 stage. Euro 5 and 6 regulations reduce the PM mass emission standard for diesel and introduce PM standards for gasoline cars with direct injection (DI) engines as well, numerically equal to those for diesel. The legislation also introduces a particulate number emission standard (P or PN) at the Euro 5/6 stage. At the time of adoption of the Euro 5/6 regulation, its mass-based PM emission limits could only be met by closed particulate filters (wall through filters). Number-based PM limits will prevent the possibility that in the future open filters are developed that meet the PM mass limit, yet enable a high number of ultrafine particles to pass.

The light-duty (LD) $NO_x$ regulations in Europe and US are compared in Fig. 1 [2]: the trend is always for very low $NO_x$ emissions. Tighter regulations are foreseen for developing markets like Brazil, China and India.

While compliance with previous $NO_x$ regulatory limits under lean conditions has been largely achieved without resort to $NO_x$ after-treatment, either selective catalytic reduction (SCR) or $NO_x$ storage reduction (NSR) need to be applied to achieve the most severe $NO_x$ standards. Indeed, with the proven technologies of automotive catalysis, the three-way catalytic (TWC) converter used for stoichiometric gasoline engines requires the absence of oxygen or very little excess oxygen and can reduce some $NO_x$ under lean conditions. An additional driver for the use

P. Forzatti (✉) · L. Lietti (✉) · L. Castoldi
Laboratory of Catalysis and Catalytic Processes and NEMAS, Dipartimento di Energia, Centre of Excellence, Politecnico di Milano, Milan, Italy
e-mail: pio.forzatti@polimi.it

L. Lietti
e-mail: luca.lietti@polimi.it

**Table 1** EU emission standards for passengers' cars (Category M), g/km

| Tier | Date | CO | $NO_x$ | HC + $NO_x$ | PM |
|---|---|---|---|---|---|
| Diesel | | | | | |
| Euro 1 | July 1992 | 2.72 | – | 0.97 | 0.14 |
| Euro 2 | January 1996 | 1.0 | – | 0.7 | 0.08 |
| Euro 3 | January 2000 | 0.64 | 0.50 | 0.56 | 0.05 |
| Euro 4 | January 2005 | 0.50 | 0.25 | 0.30 | 0.025 |
| Euro 5 | September 2009 | 0.500 | 0.180 | 0.230 | 0.005 |
| Euro 6–1 | September 2014 | 0.500 | 0.080 | 0.170 | 0.0045 |
| Petrol (gasoline) | | | | | |
| Euro 1 | July 1992 | 2.72 | – | 0.97 | – |
| Euro 2 | January 1996 | 2.2 | – | 0.5 | – |
| Euro 3 | January 2000 | 2.3 | 0.15 | – | – |
| Euro 4 | January 2005 | 1.0 | 0.08 | – | – |
| Euro 5 | September 2009 | 1.000 | 0.060 | – | 0.005 |
| Euro 6–1 | September 2014 | 1.000 | 0.060 | – | 0.0045 |

Before Euro 5, passenger vehicles > 2500 kg were type approved as light commercial vehicles $N_1$-I

of de-$NO_x$ after-treatment systems is emerging now in Europe: real world driving emissions. Investigators have found that the $NO_x$ emissions from LD diesels can be 3–5 times higher than the laboratory certification level [3]. Along these lines new test cycles (e.g. worldwide harmonized Light duty driving test cycle, WLTC) are under development that are obtained from real world data and require advanced control for cold start, steeper transients accelerations, and higher speed and load conditions. These will make the removal of $NO_x$ extremely challenging. Finally, the strategy to improve the fuel economy of cars and to reduce $CO_2$ emissions will motivate more extensive use of diesel vehicles and lean burn DI gasoline vehicles due to the more effective combustion realized under lean conditions.

The SCR approach is based on the reaction between NO and $NH_3$ [4], which is produced by hydrolysis of an aqueous urea solution injected into the exhausts from an on-board tank, according to the standard SCR reaction:

$$4\,NO + 4\,NH_3 + O_2 \rightarrow 4\,N_2 + 6\,H_2O \quad (1)$$

The activity at low temperature, where most of $NO_x$ emissions are generated, can be improved by positioning a DOC unit upstream of the SCR converter to oxidize NO to $NO_2$. This allows the occurrence of the fast SCR reaction, which is considerably faster than reaction (1) at low temperatures [5, 6]:

$$NO + NO_2 + 2\,NH_3 \rightarrow 2\,N_2 + 3\,H_2O \quad (2)$$

The first commercial use of SCR $NO_x$ control in heavy duty (HD) trucks employed traditional vanadia-tungsta-titania catalysts. Nowadays Fe- and Cu-zeolites are preferred, in view of better high-temperature durability, since the SCR catalyst receives hot gases during regeneration of the upstream diesel particulate filter (DPF), and in view of higher low temperature activity. Copper zeolite is the preferred catalyst, has the best low-T performance and shows very little sensitivity to $NO_2$ concentration. Iron zeolite has the best high-T performance but requires $NO_2$ management in the inlet gas to improve LT performance, as do vanadia catalysts. This in turn, implies a higher precious metal usage in the DOC unit.

The $NH_3$/urea SCR is recognized as the most effective technology for the abatement of $NO_x$ emissions from HD diesel vehicles, and a growing interest in the same technology is coming also from LD vehicles and passenger cars, in order to combine low fuel consumption and low $NO_x$ emissions.

The NSR, also referred to as lean $NO_x$ traps (LNT), represents an alternative viable technology for the removal of $NO_x$ under lean conditions in vehicles [7–9]. The system

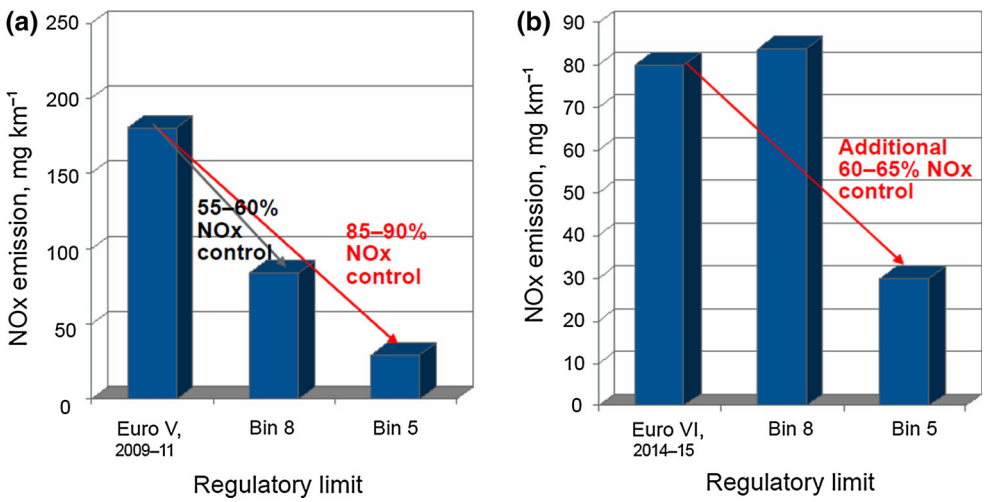


**Fig. 1** Euro V and Euro VI light-duty $NO_x$ regulatory limits compared to the U.S.: **a** About 55 to 60 % $NO_x$ control will be needed for a Euro V (2009) diesel to hit the U.S. Bin 8 maximum allowable emission (45 states). For Bin 5 (50 states) nominally 85 to 90 % $NO_x$ control is needed; **b** For Euro VI (2014), the requirement is 60 to 65 % additional $NO_x$ reduction (reprinted from [2])

is operated in a cyclic manner by alternating a long lean phase (30–90 s) and a short rich phase (3–5 s). The basic concept is that $NO_x$ are trapped onto the catalyst when the engine is running lean and are reduced to produce $N_2$ when the engine is running rich. A typical NSR catalyst comprises a noble metal such as Pt to oxidize NO, CO and unburned hydrocarbons and to reduce trapped $NO_x$, and an alkaline and/or alkaline-earth component such as barium and/or potassium to trap the $NO_x$ as nitrites/nitrates. Besides the catalysts typically contain Rh and Ce. These catalyst components are dispersed on a high surface area alumina support. The overall principle of operation of NSR has been described by the following five steps [9]: (i) oxidation of NO to $NO_2$; (ii) NO and/or $NO_2$ up-take in the form of nitrite and/or nitrates; (iii) evolution of the reducing agents when the exhaust is switched to the rich condition; (iv) $NO_x$ release from stored nitrites and nitrates; (v) reduction of released $NO_x$ to $N_2$.

The NSR technology has been commercialized for passenger cars equipped with lean burn engines in the early 2000s. In spite of the cost of the noble metal catalysts, NSR is a favored approach for lighter vehicles (i.e. engines of less than about 2.0 to 2.5 l capacity), mainly due to the fact that big layout modifications are unnecessary and the relatively fixed cost of an on-board urea system. However, since mixed-mode engines greatly reduce low-load $NO_x$, NSR systems could be operated at temperatures greater than 300 °C with a substantially lower loading of the platinum group metals (PGM). This could make NSR economically attractive for cars with mixed-mode engines of higher capacity as well (i.e. up to 5 or 6 l) [2].

The durability of LNTs to sulphur contamination has always been a major problem of NSR, based on the fact that sulphates are more stable than nitrites/nitrates and tend to poison the catalyst basic sites where $NO_x$ are adsorbed [10, 11]. Accordingly, the catalyst is typically oversized to compensate for degradation during a given period and must be periodically regenerated; this is accomplished by decomposing the sulphates at high temperature under reducing conditions to give $SO_2$ and $H_2O$ for a total of few minutes every few thousands km. In view of the introduction of ultra-low sulphur fuels, improvements in the catalyst resistance to sulphur poisoning and new control strategy, which limit the desulfation temperature, LNTs are effective to about 80 % $NO_x$ efficiency in real world Light Duty systems [12]. Attention is also paid to limit the $H_2S$ peak amount released during desulfation.

In order to decrease the size and the weight of the aftertreatment devices, integrated systems have been developed where existing complementary technologies are combined. In the LNT + SCR configuration, ammonia slipped from the LNT catalyst during the rich phase is adsorbed onto the SCR catalyst bed placed downstream. Such adsorbed $NH_3$ reacts according to the SCR reactions with upcoming $NO_x$ present in the exhausts which have not been trapped onto the NSR catalyst bed during the lean phase and with $NO_x$ released during the fast lean-rich switch that escape from the NSR catalyst bed. Accordingly, over the LNT + SCR system the $NO_x$ removal efficiency is increased, the ammonia slip is reduced and the PGM usage is lower. This technology was introduced in the US and in Europe in the 2000s [13].

Besides, in order to control soot emissions, technologies like DPF and continuously regeneration trap (CRT) [14, 15] are used in combination with SCR and LNT catalysts. Although changes to engine design will improve engine emissions in order to meet both PM and $NO_x$ regulatory limits, combined systems including PM and $NO_x$ aftertreatment can be utilized. Soot treatment, $NO_x$ reduction and CO and hydrocarbons oxidation functions are combined on a single monolith developed by Toyota and known as diesel particulate—$NO_x$ reduction (DPNR) [16]. The commercialized "4 way catalytic converters" are composed of a particulate wall-flow filter coated with an NSR catalyst layer and work under cyclic conditions, as LNT catalyst does. Particulate filter regeneration is supposed to be effective during the lean phase, due to the presence of $NO_x$ and the excess of oxygen in the exhaust gas, similarly to that occurring in the CRT technology (soot combustion by direct and cooperative reactions).

In this paper, fundamental issues of the NSR technology are addressed with the aim to provide a critical survey, and to identify open issues and space for future advancement. The reaction paths and the mechanism involved in the storage of $NO_x$ and the role of proximity between the noble metal and the alkali or alkaline-earth component of the catalyst are discussed in Sect. 2. The release of $NO_x$, the reaction pathways of $NO_x$ reduction using different reducing agents ($H_2$, CO, hydrocarbons), and the mechanisms involved in the formation of $N_2$, $NH_3$ and $N_2O$ are illustrated in Sect. 3. The use of LNT in combination with other technologies like LNT + SCR and DPNR is addressed next and key aspects that highlight the synergies of the individual technologies are discussed. Finally, the perspectives of the NSR technology are outlined.

## 2 Reaction Pathways and Mechanistic Features in the Storage of $NO_x$

### 2.1 The $NO_x$ Storage Mechanism

There is ample evidence in the literature that suggests $NO_2$ is a precursor in the storage of $NO_x$; the $NO_2$ can be gas-phase, a surface-bound precursor, or an intermediate species.

Fridell et al. [17] suggested that $NO_2$ is formed from NO oxidation and is stored onto the catalyst surface as nitrates:

$$NO + 1/2\ O_2 \rightarrow NO_2 \quad (3)$$

$$BaO + 3\ NO_2 \rightarrow Ba(NO_3)_2 + NO\uparrow \quad (4)$$

In this pathway, hereafter quoted as the nitrate route, Pt catalyses the oxidation of NO to $NO_2$ and the alkali- or alkali-earth metal compound participates in the $NO_2$ storage reaction. It is noted that reaction (4) involves the disproportionation of $NO_2$ to nitrite and nitrate intermediates, followed by the oxidation of nitrites to nitrates:

$$2\ BaO + 4\ NO_2 \rightarrow Ba(NO_3)_2 + Ba(NO_2)_2 \quad (5)$$

$$Ba(NO_2)_2 + 2\ NO_2 \rightarrow Ba(NO_3)_2 + 2\ NO\uparrow \quad (6)$$

Indeed NO is effectively oxidized to $NO_2$ over Pt, although Ba has a negative effect on the rate of NO oxidation, and NSR trapping materials sorb more effectively $NO_2$ compared to NO [9]. Besides both nitrite and nitrate ad-species have been simultaneously observed by several authors by means of FTIR at the preliminary stage of storage from $NO_2$. Nitrites eventually are oxidized to nitrates, that prevail after a sufficiently long storage period [17–20].

However spectroscopic data in the early LNT literature suggest that the formation of nitrites may precede that of nitrates during $NO/O_2$ adsorption [21, 22]. Indeed some of us have indicated another pathway for the storage from $NO/O_2$, on the basis of combined pulse reactor experiments and in situ FTIR measurements accomplished over $Pt–Ba/Al_2O_3$, $Ba/Al_2O_3$, $Pt/Al_2O_3$ catalysts and bare $Al_2O_3$ [23, 24]. This route, hereafter called the nitrite route, is based on the stepwise oxidation of NO at a Pt site followed by adsorption at a neighboring Ba site to form nitrite ad-species:

$$BaO + 2\ NO + {}^1\!/_2 O_2 \rightarrow Ba(NO_2)_2 \quad (7)$$

In this route, the cooperative action between Pt and nearby Ba sites prevents the over-oxidation of NO to $NO_2$ due to the trapping of nitrite species; nitrites can be oxidized to nitrates. In addition to the formation of nitrites, the oxidation of NO to $NO_2$ over Pt may also occur and $NO_2$ can be stored on Ba sites directly in the form of nitrates via reaction (4). A sketch of the nitrite and nitrate pathways for $NO_x$ storage is given in Fig. 2.

It is worth noting that the formation of nitrates during $NO/O_2$ uptake followed by FTIR collected in situ under static conditions may be biased by the spurious oxidation of NO to $NO_2$ in the gas phase followed by adsorption of $NO_2$; this is prevented under *operando* conditions.

Recently it has been confirmed by FTIR under *operando* conditions [20] that $NO/O_2$ adsorption on $Pt–Ba/Al_2O_3$ at low temperature results exclusively in the formation of nitrites. Indeed, as shown in Fig. 3a, the adsorption at 150 °C results in the formation of chelating nitrites with characteristic bands at 1,350 $cm^{-1}$ [$\nu_{sym}$ ($NO_2$)] and at 1,217 $cm^{-1}$ [$\nu_{asym}$ ($NO_2$)], that grow during storage. A small band at 1,544 $cm^{-1}$ is seen only at high exposure times whose assignment is still under debate (monodentate nitrites/bidentate nitrates). Besides, as shown in Fig. 3d, immediately upon admission NO is detected at the reactor exit and the formation of $NO_2$ at catalyst saturation is at most negligible. It was concluded that at low temperature (150 °C) $NO_x$ are stored only via the nitrite route in the form of nitrites.

At higher T (250 °C), as shown in Fig. 3b, the band of nitrites at 1,217 $cm^{-1}$ is observed as well, that increases with storage, goes through a maximum and then almost disappears, while the bands of nitrates at near 1,320 and 1,420 $cm^{-1}$ increase markedly. The presence of the isosbestic point in the FTIR spectra confirms that nitrites are transformed into nitrates. Besides the oxidation of NO to $NO_2$ increases and a dead time in the NO breakthrough is observed (Fig. 3e), that has been associated with the occurrence of the nitrite route and with the integral behavior of the reactor. It was concluded that in addition to the nitrite pathway, the nitrate route was also effective at this temperature (250 °C).

At 350 °C both nitrites and nitrates are formed initially (Fig. 3c). The band of nitrites at 1,217 $cm^{-1}$ disappears soon while the bands of nitrates markedly increase and are the only bands present after 10 min of exposure. Besides, the dead time in NO breakthrough is greater and the oxidation of NO to $NO_2$ is more significant at this temperature (Fig. 3f). It is noted that the storage of $NO_2$ does not allow conversion of NO to $NO_2$ to be monitored using $NO_2$ evolution until a significant amount of sorption has occurred. It was concluded that at high temperature both the nitrite and nitrate pathways are rather effective and $NO_x$ are stored only in the form of nitrates after prolonged time of exposure.

By combining the results of operando FTIR spectroscopy with those of the synchronous quantitative analysis of the gaseous species, the concentrations of nitrites and nitrates ad-species as function of time were evaluated at the quantitative level, as shown in Fig. 4. Inspection of the Figure indicates that the storage of $NO_x$ at 150 °C from $NO/O_2$ occurs exclusively through the nitrite route: in fact only nitrites are formed at this temperature, and $NO_2$ and nitrates are not observed. The nitrite route is faster at higher temperatures as well. However at 200 °C and above the nitrites are oxidized to nitrates and nitrates are also formed directly from $NO_2$ via the nitrate route. Because of this, a maximum in the concentration of nitrite species is observed. At 350 °C the maximum is smaller and is seen at shorter time of exposure. Still the nitrites prevail over the nitrates for a storage period of about 15 min at 250 °C and of a couple of minutes at 350 °C.

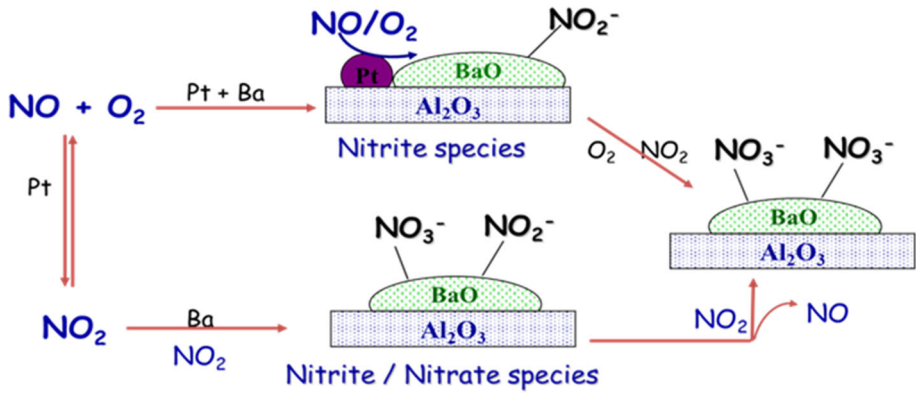


**Fig. 2** Sketch of the nitrite and nitrate routes in the process of $NO_x$ storage

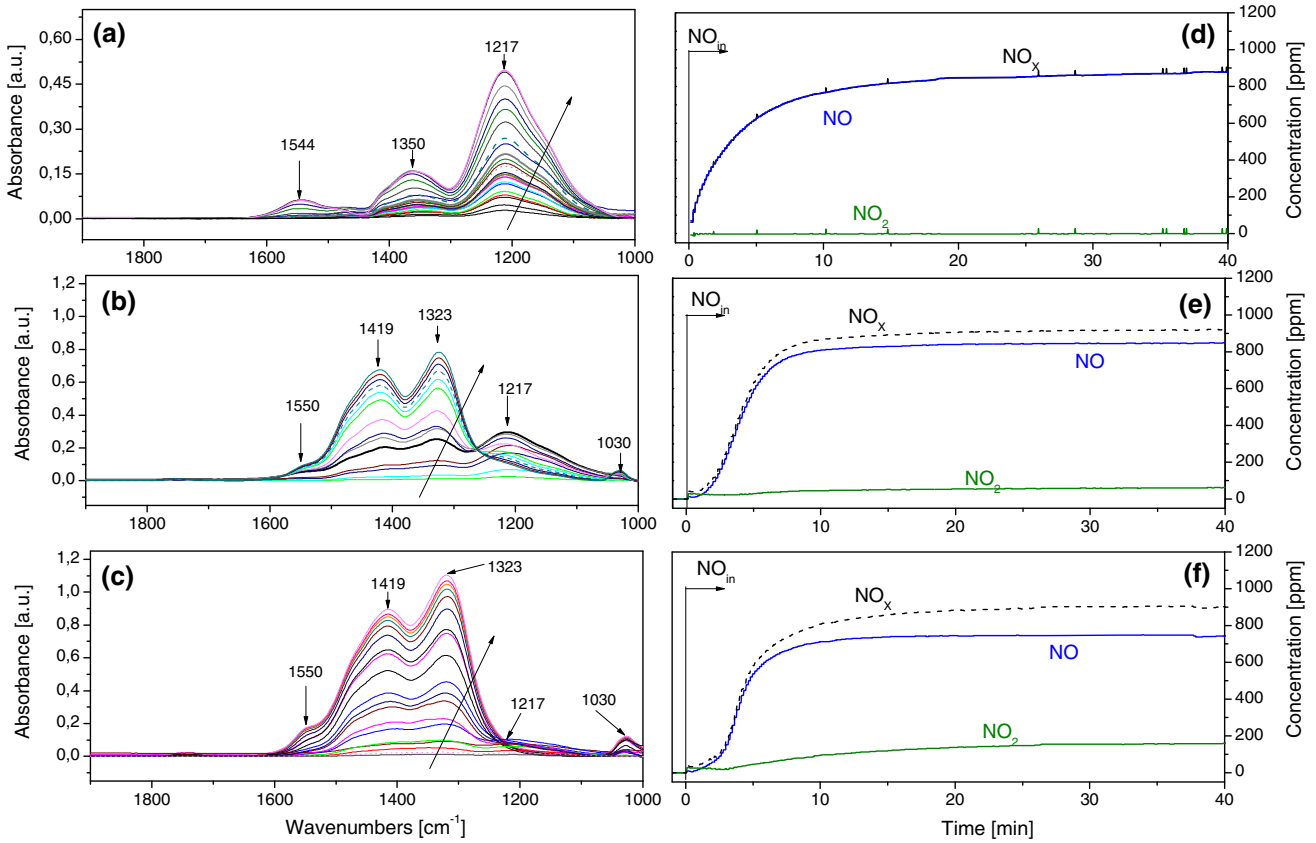


**Fig. 3** Results of operando FT-IR analysis upon $NO/O_2$ exposure (1,000 ppm NO in He + 3 % v/v $O_2$) of the model Pt–$Ba/Al_2O_3$ sample: **a** at 150 °C; **b** at 250 °C; **c** 350 °C. FT-IR spectra are recorded every 30 s (increasing storage time indicated by the *arrow* in the Figures) and the subtrahend spectrum is the catalyst before $NO/O_2$ admission. In **d–f** the gas phase analysis at the same temperature, respectively, in terms of NO, $NO_2$ and $NO_x$ is reported

The concentrations of the adsorbed species provided by operando FTIR and of the gaseous species provided by the simultaneous on line analysis of the gas phase upon exposure of Pt–$Ba/Al_2O_3$ to $NO/O_2$ mixture have been used as direct experimental responses to estimate the kinetic parameters of the steps involved in the process of $NO_x$ storage. At variance, in traditional kinetics the concentration of adsorbed species is estimated in order to gain a satisfactory fitting of the time evolution of the gaseous species. Appropriate reaction scheme, kinetic models and reactor model of the IR cell were developed. Considering the fact that this approach is the result of the joint application of spectroscopic and kinetic methods, it has been termed as spectro-kinetics. The model was found to fit nicely with the

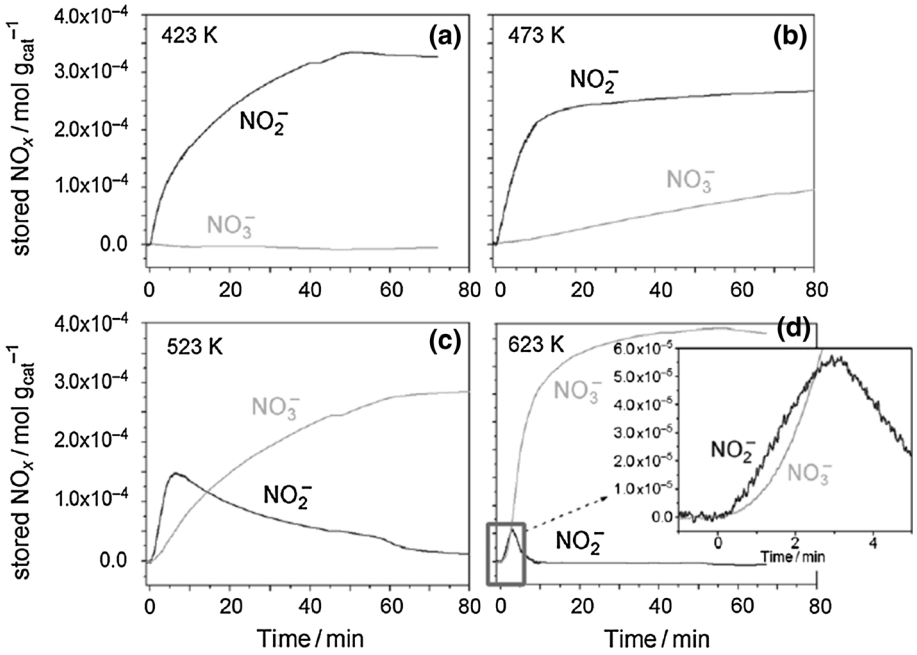


**Fig. 4** Evolution versus time of the main bands for different surface species detected by using FT-IR spectroscopy under operando conditions upon NO/$O_2$ exposure (1,000 ppm NO in He + 3 % v/v $O_2$) at 150, 200, 250 and 350 °C of the model Pt–Ba/$Al_2O_3$ sample (reprinted from [20])

time evolution of the concentration of NO and $NO_2$ in the gas phase and the surface coverage of nitrites and nitrates in the investigated temperature range [25].

The effect of $CO_2$ and $H_2O$, that are present in the exhausts, on $NO_x$ storage over Pt–Ba/$Al_2O_3$ has been addressed recently in our labs [26], and among others by Weiss et al. [27], Epling et al. [28] and by Chaugule et al. [29]. We found that the nitrites pathway is not significantly affected by the presence of $CO_2$ at low temperature, but is inhibited at higher temperatures. However, the nitrate pathway is inhibited as well, particularly at high temperature, but to a lower extent. The different inhibiting effect of $CO_2$ has been ascribed to the different relative thermal stability of carbonates, nitrites and nitrates as function of temperature, which has been evaluated by means of dedicated adsorption–desorption experiments. The effect of water was minor, because $BaCO_3$ is more stable than $Ba(OH)_2$ [30, 31]. It is concluded that nitrites are formed preferentially during the early period of $NO_x$ storage from NO/$O_2$ also in the presence of $CO_2$ and $H_2O$.

### 2.2 Relevance of the Proximity Between the Noble Metal and the Alkali or Alkaline-Earth Component

To investigate the importance of close contact between Pt and BaO during the storage, Cant et co-workers compared the $NO_x$ storage characteristics of four systems: BaO/$Al_2O_3$, a sequential system with Pt/$SiO_2$ ahead of BaO/$Al_2O_3$, a combined system with Pt/$SiO_2$ and BaO/$Al_2O_3$ physically mixed, and BaO/$Al_2O_3$ with Pt deposited on it [32]. They found that storage of $NO_x$ from NO/$O_2$ by the Pt–BaO/$Al_2O_3$ sample differed from that of the sequential and combined systems. Indeed, the rate of storage on Pt–BaO/$Al_2O_3$ is faster, and the total storage capacity under the conditions used is attained more quickly. The implication is that Pt, in close proximity to BaO, either allows uptake of NO or $NO_2$ in a way that is not feasible when Pt is absent or enables conversion of $NO_x$ to nitrites/nitrate as storage proceeds. Spillover of $NO_2$ from Pt to BaO/$Al_2O_3$ is one way in which the latter might occur. These authors also investigated the isotopic exchange between $^{15}NO$ and stored $^{14}NO_x$. The rate of exchange was more than five times as fast for Pt/BaO/$Al_2O_3$ than for the combined Pt/$SiO_2$ + Ba/$Al_2O_3$ system, demonstrating spillover of $NO_x$ species between Pt and Ba in close proximity.

Similar results have been reported by Nova et al. [33]. Indeed, comparing the results between the physical mixture made of Pt/γ-$Al_2O_3$ and Ba/γ-$Al_2O_3$ and the ternary Pt–Ba/γ-$Al_2O_3$ sample it clearly appeared that the two systems are characterized by a similar $NO_x$ breakthrough time but the physical mixture presents a higher oxidizing capacity, as revealed by the higher conversion of NO to $NO_2$ measured at catalyst saturation. In addition, the physical mixture resulted able to adsorb significant amounts of $NO_x$. It was assumed that the mechanism of $NO_x$ adsorption operating on the physical mixture, i.e. in the absence of interaction between Pt and Ba atoms, is the nitrate route: NO is oxidized to $NO_2$ on Pt sites (reaction (3)) and then is adsorbed on Ba (and Al sites) via the disproportionation reaction (reaction (4)). NO, which is released during the same reaction is re-oxidized to $NO_2$ and this results in a significant delay in the $NO_x$ breakthrough also in this case.

Hence, the data on the physical mixture confirm the feasibility of the $NO_x$ storage mechanism proposed in the literature implying the oxidation of NO to $NO_2$ followed by $NO_2$ adsorption on the catalyst surface to form nitrates. In this case, no direct interaction is necessary to have an effective $NO_x$ uptake. However, this is not the case of representative NSR catalysts, in which Pt and Ba are on the same support and which must be able to catalyze the reduction of the stored $NO_x$, as indeed realized in the NSR technology. As a matter of fact, the physical mixtures made of $Pt/SiO_2$ and $Ba/Al_2O_3$ or $Pt/Al_2O_3$ and $Ba/Al_2O_3$ are active towards the $NO_x$ reduction at considerably higher temperatures compared to the ternary system $Pt–Ba/Al_2O_3$ [32, 33]. This is consistent with the decomposition of stored $NO_x$ to gaseous $NO_x$ and subsequent reduction by a catalytic reaction on Pt particles located remotely from BaO.

To investigate this interaction further and to better understand its role in the storage mechanism, a study was undertaken by Castoldi et al. [34] using $Pt–Ba/Al_2O_3$ samples with different Ba loadings, in order to vary the number of Pt–Ba neighboring couples. The CO chemisorption measurements performed by means of in situ FTIR analysis showed the characteristic band of CO linearly adsorbed on Pt sites in all cases; however, upon increasing the Ba loading the band progressively shifts towards lower energy due to the increase of the catalyst basic character. Hence, the data indicate a strong interaction between Pt and the basic oxygen anions of the Ba phase, suggesting that the exposed Pt sites and the Ba component are in close proximity. In addition, it has been shown that when applying a rectangular step feed of NO in $He + O_2$ (3 % v/v) both the $NO_x$ breakthrough and the storage capacity of the catalyst increase with the Ba content not only because of the amount of Ba, but also the number of Pt-neighboring Ba sites increase, the uptake of $NO/O_2$ is faster over these sites and a large percentage of Ba participates to NSR [34]. The fraction of Ba that participates in the storage process ("active" Ba) increases linearly with the catalyst Ba content passing through a maximum that represents the best exploitation of the Ba component, while the Pt dispersion decreases from 80 to 40 % [34].

The relevance of the Pt–Ba proximity in the storage of $NO_x$ implies that Ba sites distant from Pt are less reactive in the storage. This eventually accounts for the slower uptake of $NO_x$ which is observed at the later stages of the trapping process, and that was explained invoking a nitrate spillover type mechanism [35, 36]. In fact the adsorption sites near Pt react and saturate first, then the trapping rate slows due to increasing resistance to nitrate surface diffusion as the N-species build around the Pt particles (two dimensional shrinking core model) and/or into the inner core of the Ba particles (three dimensional shrinking core model). The close proximity between Pt and BaO facilitate the removal of stored $NO_x$ as well by lowering the stability of adsorbed species.

## 3 Reaction Pathways and Mechanism in the Reduction of the Stored $NO_x$

There are three methods for introduction/generation of the reductant in NSR [9]. The first strategy is the DI of the fuel into the exhausts upstream of the catalyst during the rich event. In the second strategy, the fuel is continuously processed over a reformer or other devices such as plasma or a partial oxidation catalyst to generate reductants, which are more effective in accomplishing the regeneration of the $NO_x$ trap. In the third strategy, the lean burn engine is operated to generate intermittent pulses of rich exhausts to the LNT catalyst that either directly contain the reductant or are processed by the NSR catalyst or by an upstream catalyst to form the reductant. In this case, the regeneration event involves a rich transient originating from the engine.

It is difficult to determine what exact reducing species participates in the $NO_x$ reduction process since the original reductant may undergo substantial changes over the NSR catalyst or the reformed devices added upstream. Besides, extensive heat is evolved due to catalytic combustion of the reductant during regeneration events in some modes of operation. Accordingly, the catalyst operation is highly non isothermal, resulting in complex dynamic temperature distribution profiles. Temperature swings, measured as gas phase temperature changes, can be as high as 50–100 °C at the front of the catalyst and only 2–3 °C at the back of the catalyst [9]. Keeping in mind these aspects, it is obvious how complex the mechanism of reduction is for the stored $NO_x$.

### 3.1 The Release of $NO_x$

It is a common belief that the reduction of stored $NO_x$ over LNT catalysts implies the release of $NO_x$ from the catalyst surface, followed by the reduction to $N_2$ and other by-products such as $NH_3$ and $N_2O$. The process of $NO_x$ release is most commonly discussed in terms of the breakthrough of desorbed and unconverted $NO_x$ during the rich event as schematically shown in Fig. 5. However, the detailed mechanism of the release of $NO_x$ and of their further reduction remains under debate.

Some authors [37, 38] proposed that the $NO_x$ are released as a result of the heat generated by the exothermic reactions upon the lean/rich switch (thermal release). Indeed, as the rich front passes over the catalyst and the surface temperature increases, stored $NO_x$ can be released because their stability decreases with increasing temperature. However it has been shown that the reduction process,

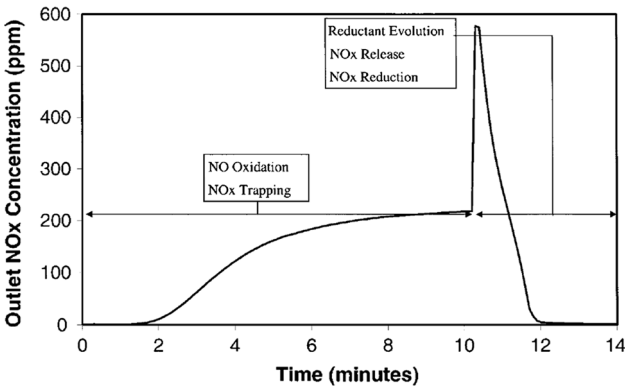


**Fig. 5** A representative $NO_x$ breakthrough and release profile. The catalyst was $Pt/Ba/Al_2O_3$,the reactant gas contained 250 ppm NO, 8 % $H_2O$, 8 % $CO_2$, 8 % $O_2$, balance $N_2$ in the lean/trapping phase and 2,000 ppm $H_2$, 8 % $H_2O$, 8 % $CO_2$, and a balance of $N_2$ in the regeneration/rich phase. The space velocity was 25,000 $h^{-1}$. The outlet $NO_x$ concentration was monitored with a chemiluminescence detector (reprinted with permission from [9])

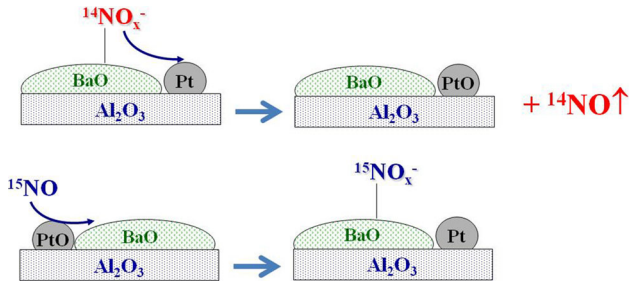


**Fig. 6** Sketch of the mechanism of NO isotopic exchange/$NO_x$ release

even when accomplished under nearly isothermal conditions (i.e. with small concentration of the reductant), occurs at temperatures well below that at which stored $NO_x$ thermally decompose. Accordingly, under these conditions, the process is not initiated by the thermal decomposition of stored nitrates, but rather by a catalytic pathway involving Pt [33]. Other authors [39, 40] have proposed that the release of $NO_x$ is caused by a decrease in the equilibrium stability of the stored nitrates due to the decrease in the partial pressure of NO and/or of oxygen upon the lean/rich switch. However this contribution is small during typical NSR operation since only a negligible desorption of weakly adsorbed $NO_x$ species was observed in the time range of few seconds characteristic of the rich period, when the NO feed and the $O_2$ feed were shut down after the storage of $NO_x$ was completed [30, 33]. Finally, the release of $NO_x$ may be promoted by the establishment of a net reducing environment [41, 42].

To account for the reduction of $NO_x$ either the reverse spill-over of $NO_x$ from Ba to Pt is occurring or alternatively the reductant activates and then spills over from Pt sites to the storage component and reacts directly with nitrites and nitrates, so that they are eventually released as $NO_x$ [32, 43, 44]. The subsequent reduction of the released $NO_x$ may occur at the Pt metal sites following a TWC-like chemistry [45]. The transient product distribution displayed by three catalysts having varied dispersions (3.2, 8 and 50 %) was described by Harold and coworkers [35, 46] using a model based on global kinetics and detailed crystallite-scale catalyst features and was explained by the localized stored $NO_x$ gradients in the Ba phase. The rate determining process during the regeneration was found to be the diffusion of stored $NO_x$ within the Ba phase towards the Pt/Ba interface. Indeed the results reported by Coronado and Anderson [47], Cant et al. [32] and Nova et al. [33] clearly show that $NO_x$ decomposition is easier when Pt and Ba are in close proximity.

Even if the net $NO_x$ release at the lean/rich interface represents a small loss under many of the operating conditions, this release increases at higher temperatures and can result in not attaining the required emissions standards. Therefore, one of the most important issues is understanding the pure contributes that cause the $NO_x$ release and the selectivity to $N_2$. Although the proposed pathways of $NO_x$ release are relatively well accepted, decoupling the release of $NO_x$ from their subsequent reduction to $N_2$ or other products is not possible during typical NSR operation. Indeed, in the presence of a reducing agent the $NO_x$ release is immediately followed by reduction of the released $NO_x$, which is a very fast reaction. However, recently the release of stored $NO_x$ has been decoupled from the reduction of the released $NO_x$ and measured by performing NO isotopic exchange experiments under temperature programming, using labelled gaseous $^{15}NO$ and unlabelled $^{14}NO_x$ stored on the $Pt–Ba/Al_2O_3$ catalyst. The exchange between gaseous $^{15}NO$ and stored $^{14}NO_x$ was previously used by Cant et al. [32] to probe the forward and reverse spillover of $NO_x$ species between Pt and BaO.

NO isotopic exchange experiments have shown that [48]: (i) Pt is necessary for the exchange because this is observed over $Pt–Ba/Al_2O_3$ but not over $Ba/Al_2O_3$; (ii) the NO isotopic exchange implies the release of stored $NO_x$ and is observed from a temperature well below that of thermal decomposition of stored $NO_x$, thus pointing to a Pt-catalysed process. The exchange is observed from about 50 °C for nitrites stored from $NO/O_2$ at 150 °C and from about 250 °C for nitrates stored from $NO/O_2$ at 350 °C; (iii) all stored $NO_x$ have been exchanged after T programming up to 350 °C and subsequent hold at this temperature for half an hour so that both nitrites and nitrates migrate between Pt and Ba sites.

The mechanism of NO isotopic exchange is sketched in Fig. 6. Upon interaction of unlabelled stored nitrite or

nitrate species with reduced Pt sites unlabelled NO is released in the gas phase and PtO species are formed. PtO species oxidize labelled NO present in the gas phase to give labelled nitrite and nitrate adsorbed species restoring the reduced Pt sites. The NO isotopic exchange is a redox process. The reduced Pt sites activate $NO_x$ stored species that are destabilized and eventually released as NO in the gas phase. It is worth to note that during typical NSR operation stored $NO_x$ upon activation could either react with the reducing agents present in the exhausts to give $N_2O/N_2/NH_3$ or produce released but unconverted NO.

It is worth noting that in the NO isotopic exchange process labelled NO represents the reducing agent so that the released unlabelled NO cannot be reduced further. For this reasons, in NO isotopic exchange experiments the release of stored $NO_x$ could be decoupled from its further reduction and the process of $NO_x$ release could be characterized unambiguously.

### 3.2 Pathways of the Reduction of Stored $NO_x$ Using $H_2$

The regeneration of the $NO_x$ storage component is a crucial phase of the NSR process. The regeneration has been studied by several authors using $H_2$ as the reductant: the formation of $NH_3$, $N_2O$ and $N_2$ was observed depending on temperature, $H_2$ concentration, time of exposure to the reductant.

Harold and coworkers [49] on the basis of measurements performed with different catalyst length sections proposed that there are two primary competing routes to the desired $N_2$ product: a direct route from the reduction of stored $NO_x$ by $H_2$ ($H_2 + NO_x \rightarrow N_2$) and a sequential route of stored $NO_x$ reacting with $H_2$ forming $NH_3$ and then $NH_3$ reducing $NO_x$ stored downstream to give $N_2$ ($H_2 + NO_x \rightarrow NH_3$; $NH_3 + NO_x \rightarrow N_2$). Evidence for the direct route and the sequential route with ammonia as intermediate has also been provided by means of in situ measurements for the transient intra catalyst species ($H_2$, $NH_3$, $N_2$, $NO_x$) using spatially resolved capillary inlet mass spectrometry (SpaciMS), which provides a spatiotemporal resolution during NSR catalyst regeneration as shown in Fig. 7 [50]. While the data clearly prove that intermediate $NH_3$ plays a significant role in LNT catalyst regeneration, it was further recognized that experimental and numerical work are needed to more clearly understand the partitioning between the two suggested regeneration pathways, the direct route and the sequential route with ammonia as intermediate.

Lindholm et al. [31] showed that $N_2O$ and $NH_3$ can be formed when reducing $NO_x$ with $H_2$ and that NO reduction, $NH_3$ formation and $N_2O$ formation depend on the $H_2$ concentration. A delay in the ammonia signal was observed and was explained by the SCR-type reaction between nitrites/nitrates adsorbed on the storage component and ammonia; when the coverage of nitrites/nitrates has decreased $NH_3$ is observed in the gas phase.

Ribeiro et al. [51, 52] proposed that the regeneration of $Pt–Ba/Al_2O_3$ monolith $NO_x$ trap with hydrogen involves a localized reaction front of the reductant that travels through the catalyst bed with complete regeneration of the trapping sites. The process was limited by the supply of the hydrogen atoms, irrespective of the source of hydrogen ($H_2$ or $NH_3$), and occurred through a complex pathway where at first nitrogen and ammonia were formed according to a parallel scheme. $NH_3$ further reacts with the stored $NO_x$ leading to the selective formation of $N_2$.

In order to elucidate the mechanism governing the reduction of the $NO_x$ species stored onto a model $Pt–Ba/Al_2O_3$ LNT catalyst in the form of nitrates, TPD (temperature programmed desorption), $H_2$-TPSR (temperature programmed surface reaction), $NH_3$-TPSR, $H_2$-ICSC (isothermal concentration step change) and $NH_3$-ICSC experiments have been performed by Lietti et al. [33, 53, 54] under nearly isothermal conditions by using a small concentration of the reductant. The data in Fig. 8 show that the reduction of stored $NO_x$ is active at temperatures well below that of $NO_x$ thermal decomposition (near 120 °C in panel B vs. near 330 °C in panel A) and accordingly the $NO_x$ reduction is a Pt-catalyzed process that does not require the thermal release of stored $NO_x$ as the preliminary step. Besides, Fig. 8 shows that the reduction of nitrates by $H_2$ occurs from much lower temperature in the presence than in the absence of $H_2O$ (near 50 °C in panel C vs. near 120 °C in panel B). The promoting effect of water might be explained considering that water increases the $H_2$ spillover rate over oxide surfaces [55], thus enhancing the reduction of nitrates stored far away from Pt sites. However specific effects of water on the mobility and reactivity of adsorbed nitrates can be suggested as well considering that water affects the features of nitrate adspecies, as reported by Szanyi and coworkers [56]. This is in line with mechanism involving the $NO_x$ spillover from Ba to Pt sites. From Fig. 8 it is also clear that the reduction of nitrates by $H_2$ results in the formation of ammonia as the main product when accomplished at low temperatures (panel C) as opposed to when it's carried out at high temperatures (e.g. 350 °C). Indeed, in this case $N_2$ represents the most abundant reaction product and $NH_3$ is detected in small amounts and only after $N_2$ evolution (not shown in Fig. 8). Finally, Fig. 8 shows that the reduction of nitrates by ammonia is slower since the onset of this reaction is observed at higher temperature than the one with hydrogen (near 125 °C in panel D vs. near 50 °C in panels C), and is fully selective to nitrogen (panel D).

These data were described by the following molecular reaction scheme:

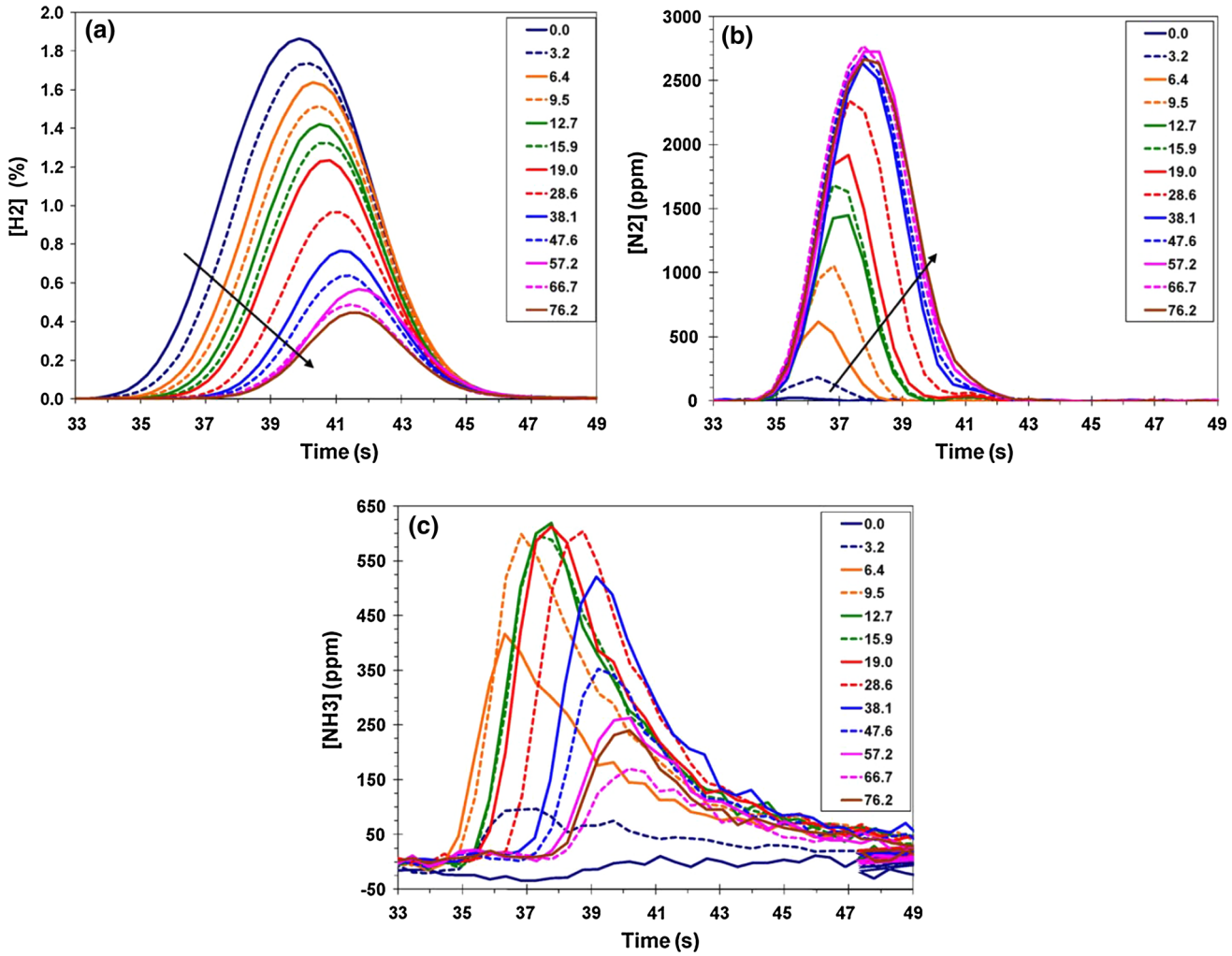


**Fig. 7** Species transients at different locations through the catalyst for **a** $H_2$, **b** $N_2$ and **c** $NH_3$ at 200 °C. The legend indicates the specific measurement location in millimeters relative to the catalyst inlet face. (reprinted with permission from [50])

$$Ba(NO_3)_2 + 8\ H_2 \rightarrow 2\ NH_3 + BaO + 5\ H_2O \quad (8)$$

$$3\ Ba(NO_3)_2 + 10\ NH_3 \rightarrow 8\ N_2 + 3\ BaO + 15\ H_2O \quad (9)$$

where reaction (8) is faster than reaction (9).

This scheme together with the integral behavior of the laboratory micro-reactor accounts for the temporal evolution of the products observed during the reduction of the stored nitrates with $H_2$ and with $NH_3$ in the investigated T range 150–350 °C. It also implies the full consumption of $H_2$ and the formation of a hydrogen front travelling along the reactor axis, with ammonia formation that occurs at the $H_2$ front. Although the data could be explained at the quantitative level by the consecutive pathway provided by reactions (8) and (9) [57] a parallel + consecutive reaction scheme, where $N_2$ is also formed directly from nitrates, cannot be ruled out.

A schematic of the regeneration pathway proposed by Ribeiro et al. [51, 52] (and by Phil et al. [58]) is depicted in Fig. 9. The Figure illustrates the propagation of the reductant front along the catalyst bed with complete regeneration of the trap. Once $NO_x$ is released it reacts with $H_2$ over Pt to form $NH_3$, $N_2$ and $N_2O$, the selectivity to the individual species depending on the local $NO_x/H_2$ concentration ratios. In the beginning of the front where the $H_2$ level is high compared to the $NO_x$ $NH_3$ will be mostly formed. The $NH_3$ formed will further react with more $NO_x$ to give either $N_2$ or $N_2O$ if the temperature is sufficiently high. If the $N_2O$ is formed behind the front, it will be reduced to $N_2$ by $H_2$ or $NH_3$. As the front approaches the end of the catalyst the supply of $NO_x$ starts to deplete and is insufficient to react with the $NH_3$ formed upstream, leading to the $NH_3$ breakthrough. Before the reaction front reaches the end of the bed, most of the non-selective products will react further to form $N_2$ and maintain the high selectivity of the overall NSR catalyst.

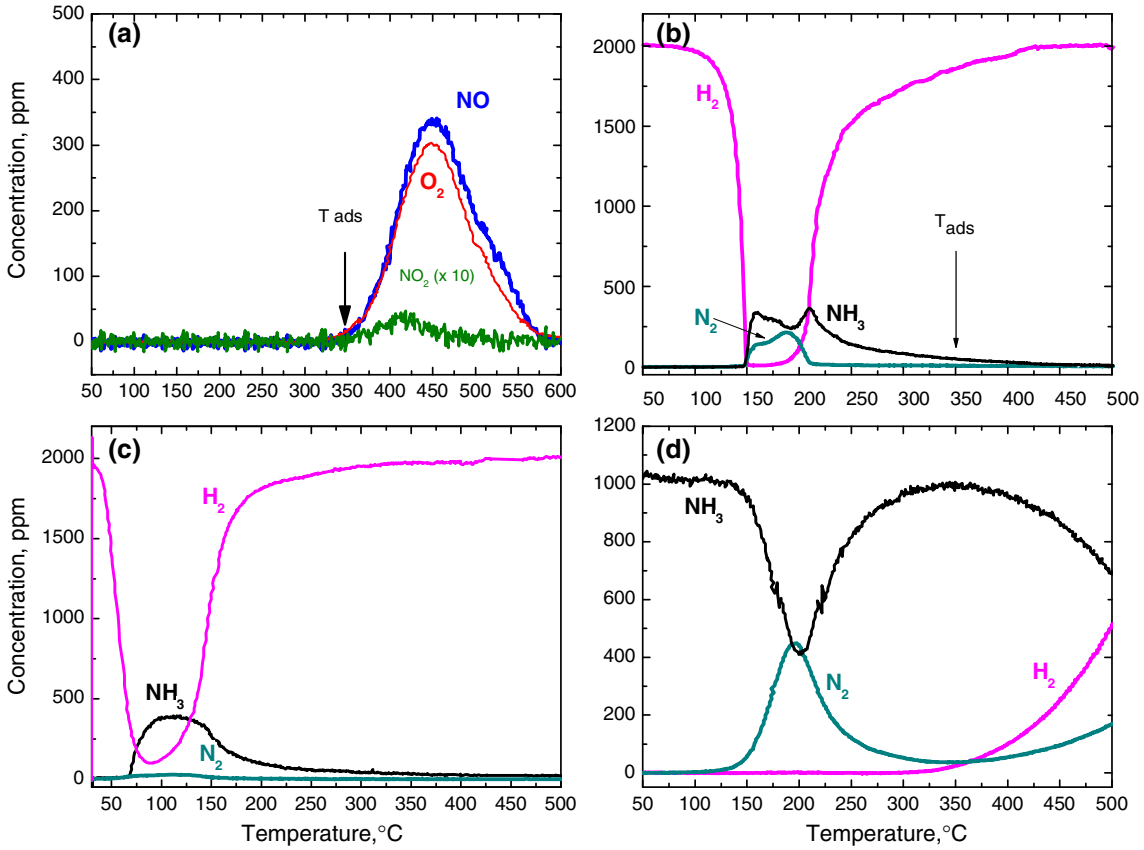


**Fig. 8** **a** TPD in He from r.t. to 600 °C (10 °C/min); **b** $H_2$-TPSR (2,000 ppm $H_2$) from r.t. to 500 °C (10 °C/min); **c** $H_2 + H_2O$-TPSR (2,000 ppm $H_2$ + 1 % v/v $H_2O$) from r.t. to 500 °C (10 °C/min); **d** $NH_3 + H_2O$-TPSR (1,000 ppm $NH_3$ + 1 % v/v $H_2O$) from r.t. to 500 °C (10 °C/min). Storage conditions: 1,000 ppm NO in 3 % v/v $O_2$ + He at 350 °C over Pt–Ba/$Al_2O_3$ catalyst

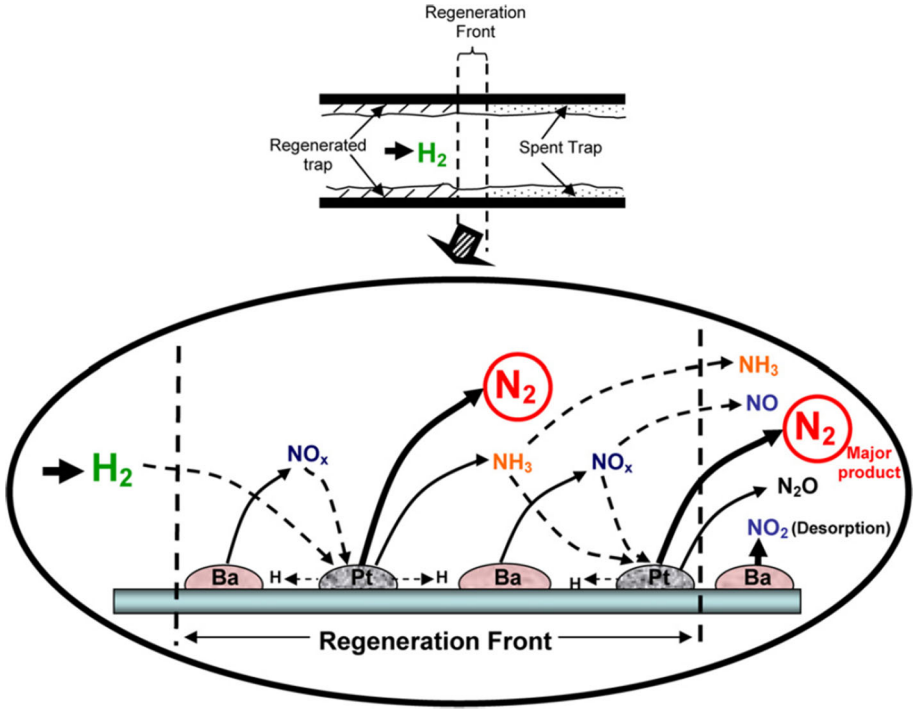


**Fig. 9** Schematic of the reduction mechanism for a Pt/BaO/$Al_2O_3$ monolith regenerated with $H_2$. Bottom panel illustrates a zoomed-in picture of the reaction front (reprinted with permission from [52])

### 3.3 Pathways of $NO_x$ Reduction Using CO and Hydrocarbons

The regeneration of LNT catalysts has also been studied using CO, propane, propene and other hydrocarbons as reductants [56, 59–61]. It has been observed that $H_2$ and CO are highly efficient reductants compared to $C_3H_6$, which is somewhat less efficient. $C_3H_8$ did not show any $NO_x$ reduction ability for $NO_x$ stored on $Pt/Ba/Al_2O_3$ except at 350 °C.

Szailer et al. [56] reported that during the reduction by CO of $NO_x$ stored on $Pt/Al_2O_3$ and $Pt–Ba/Al_2O_3$ at low temperature and under dry conditions stable isocyanates form at the Pt particles and spill over the basic oxide component of the catalyst, resulting in consumption of a large fraction of gas-phase CO and formation of a significant amount of $CO_2$ but not of $N_2$. At temperatures corresponding to the onset of stored nitrate decomposition these NCO species can readily react with the $NO_x$ released by the catalyst to give $N_2$ and $CO_2$ according to the reaction:

$$NCO + NO_x \rightarrow N_2 + CO_2 \quad (10)$$

$N_2$ formation was significantly enhanced by adding water to the NCO covered catalysts because NCO was hydrolyzed to $NH_3$ and $CO_2$ so that the formed $NH_3$ could react with $NO_x$ and form the intermediate that eventually generated $N_2$ and $H_2O$.

Forzatti et al. [62] showed that the reduction of nitrates stored onto $Pt–Ba/Al_2O_3$ by CO under dry conditions does not involve the thermal release of stored $NO_x$ as the preliminary step, is seen from a temperature where Pt-carbonyls disappear and CO is consumed while $N_2$ is observed from a slightly higher temperature. It was found that the reduction of nitrates by CO occurs via a consecutive reaction scheme with formation of NCO species followed by reaction of these species with nitrates/nitrites and that the reaction of NCO species to give nitrogen is slower than the reduction of nitrates with CO to give NCO species. Large amounts of stable NCO species were formed and retained onto the catalyst surface at the end of the rich phase and were oxidized to give $N_2$ during the subsequent lean phase upon admission of $O_2$ and $NO/O_2$. Lower amounts of isocyanate species were left at the end of the reduction over $Pt-K/Al_2O_3$ than over $Pt–Ba/Al_2O_3$ likely due their higher mobility [63, 64]. It is worth noting that the C and N balances during the rich and the lean phases of the NSR cycle are consistent with the formation of stable NCO species and their consumption to give $N_2$ respectively. Amiridis and coworkers [61] confirmed that the reaction of surface isocyanates with $O_2$ and NO accounts for a significant fraction of the overall $N_2$ production. The oxidation of isocyanates/cyanates with $O_2$ to give $N_2$ and $CO_2$ was observed previously over $Pt–Rh/Ba/Al_2O_3$ and $Ag/Al_2O_3$ catalysts by Daturi and coworkers [65, 66] using FT-IR spectroscopy and by Schoulten and coworkers [67] over $Pt–Ba/Al_2O_3$ performing lean–rich cycling experiments. Also Toops and coworkers [68] found that Ba–NCO is directly derived from the reduction of Ba nitrate by CO, i.e., Ba–NCO species represent a critical intermediate in the reduction of stored $NO_x$ with CO. Under dry cycling conditions with CO as the reductant, $N_2$ is mainly generated via NCO reaction with NO + $O_2$ after the switch to lean phase conditions, rather than being formed during the rich phase. However, the evolution of DRIFT spectra under both temperature-programmed and isothermal reaction modes revealed that $H_2O$ is the most reactive species with respect to isocyanate of those tested ($H_2O$, $O_2$, NO, $NO/O_2$).

The role of surface isocyanate species as intermediate in the formation of $N_2$ is also supported by previous literature reports where isocyanates formed on several HC-SCR catalysts were found to be highly reactive towards $NO_2$ and NO + $O_2$ to yield $N_2$ [69–72]. It is worth noting that NCO species are stabilized in the regeneration of NSR catalyst by CO due to the interaction with the alkali or alkaline-earth component of the catalyst.

However, different routes may be active in the reduction of stored $NO_x$ species by CO under wet conditions. Indeed the onset temperature for the CO consumption is observed at temperatures slightly lower under wet than under dry conditions and is very close to the onset temperature of the WGS reaction, the $NO_x$ removal efficiency is higher, and $NH_3$ and $H_2$ are seen among the products [73]. FTIR showed that bidentate nitrates are transformed with temperature into ionic nitrates while NCO species are observed only in small amounts. The hydrolysis of the surface NCO species to give ammonia and carbon dioxide has also been reported by Daturi and coworkers [65] and the formation of small amounts of NCO species during cycling experiments in the presence of water was observed by Amiridis and coworkers [61]. Therefore, it is concluded that hydrogen formed through the water gas shift (WGS) and/or ammonia formed by hydrolysis of NCO species could be involved in the reduction of stored $NO_x$ by CO in the presence of water. Recently Harold and co-workers [74] provided evidence that the surface NCO species are important reaction intermediates at moderate to higher temperatures (≥250 °C) during the cyclic reduction of $NO_x$ by CO under wet conditions. Current on-going spatiotemporal studies have been anticipated to identify the best routes to $N_2$.

Propylene and n-heptane were also used in the regeneration of LNT catalysts under dry conditions [35, 75]. Both propylene and n-heptane were found to react well below the onset temperature of nitrate thermal decomposition. Hence, also in this case, as in the case of $H_2$ and CO, the reduction of the stored $NO_x$ does not imply the

preliminary thermal decomposition of the $NO_x$ adsorbed species. The reduction of the stored nitrates is accompanied by the evolution of $N_2$ that represents the main product, and then of minor amounts of ammonia.

However, in reality the NSR is performed in the presence of water and it is commonly accepted that the reduction of stored $NO_x$ occurs thanks to the production of $H_2$ via steam-reforming of the hydrocarbon employed as reductant. Then *n*-$C_7$-TPSR run in the presence of water has been carried out and the onset of the nitrate reduction was observed at temperatures very close to that measured under dry conditions (200–250 °C), i.e. the reaction was not significantly affected by the presence of water. Also the distribution of reduction products was very similar.

Dedicated n-heptane steam-reforming (SR) experiments have been performed, which showed the formation of $H_2$ and $CO_2$ above 250 °C although with poor reactivity. In the SR experiments, the production of $H_2$ is observed from 250 °C. However, the amount of $H_2$ produced via the SR reaction was not sufficient to justify the large amount of $N_2$ produced. Besides no N-containing surface species, in particular isocyanates, could be detected by in situ FT-IR. Accordingly, a different pathway should likely be considered. The pathway may imply cleaning of the Pt sites by the reductant followed by migration-decomposition of the stored $NO_x$ at the reduced Pt sites.

### 3.4 Mechanism of the Reduction of Stored $NO_x$ by $NH_3$

As already mentioned, ammonia is seen among the products during reduction of stored $NO_x$ in particular at low T when hydrogen is used as reductant and it has been suggested in the literature as intermediate in the production of nitrogen. However, the mechanism of the reduction of stored $NO_x$ by $NH_3$ has not been completely clarified so far. A study has been carried out recently in our labs to identify the possible mechanism for $N_2$ formation when ammonia represents the reducing agent of the stored $NO_x$.

Considering that the NSR catalysts have been derived from classical three-way catalysts by adding an alkaline component to the active wash-coat layer, and that during the regeneration of NSR systems $NO_x$ are released in the gas phase as NO, one can suppose that a TWC-like reduction chemistry occurs. Accordingly, the following set of elementary reactions can be considered for the reaction between $NH_3$ and NO over Pt-based catalysts, as suggested in the literature [76]:

$$NO + Pt \rightarrow Pt\text{-}NO \quad (11)$$

$$Pt\text{-}NO + Pt \rightarrow Pt\text{-}N + Pt\text{-}O \quad (12)$$

$$NH_3 + Pt \rightarrow Pt\text{-}NH_3 \quad (13)$$

$$Pt\text{-}NH_3 + Pt \rightarrow Pt\text{-}H + Pt\text{-}NH_2 \quad (14a)$$

$$Pt\text{-}NH_2 + Pt \rightarrow Pt\text{-}H + Pt\text{-}NH \quad (14b)$$

$$Pt\text{-}NH + Pt \rightarrow Pt\text{-}N + Pt\text{-}H \quad (14c)$$

$$Pt\text{-}N + Pt\text{-}N \rightarrow N_2 + 2\ Pt \quad (15)$$

$$Pt\text{-}O + 2\ Pt\text{-}H \rightarrow H_2O + 3\ Pt \quad (16)$$

In this scheme gaseous NO dissociates at Pt sites cleaned by the reductant to form Pt-N and Pt-O species (reactions 11 and 12). Activation of ammonia leads to the formation of Pt-H species (reactions 14) that scavenge the O-ad-atoms leading to the formation of reduced Pt sites and water (reaction 16). The recombination of adsorbed nitrogen atoms follows to form $N_2$ (reaction 15) while reaction of adsorbed nitrogen and hydrogen atoms produces $NH_x$ and ultimately $NH_3$ (reverse reactions 14 and 13).

The mechanism of the reduction by ammonia of nitrates stored onto a Pt–$Ba/Al_2O_3$ catalyst has been investigated recently using labelled nitrates and unlabelled ammonia [77, 78]. Since in real automobile operation NO will also be present, it is of interest to study how its presence modifies the reaction network for stored $NO_x$ reduction to $N_2$, by feeding NO together with the reductant in the regeneration period. To do this, $NH_3$-TPSR and $NH_3$-ICSC of stored nitrates in the presence and absence of NO in the gas phase have been accomplished. The temperature programmed reaction (TPR) between gaseous labelled $^{15}NO$ and unlabelled $^{14}NH_3$ over Pt–$Ba/Al_2O_3$ was also studied for comparison purposes.

The results of the TPR run between $^{15}NO$ and $^{14}NH_3$ are shown in Fig. 10, panel A. The reaction is observed starting near 100 °C, with formation of single- and double-labeled $N_2O$, and of single labeled $N_2$. Above 160–180 °C the conversion of NO is complete, a drop in the concentration of $N_2O$ is observed and the reaction becomes fully selective to $N_2$. All $N_2$ isotopes are seen above this temperature, with abundances that do not change significantly with temperature. Notably, the relative abundance of the di-nitrogen isotopes observed at T > 160–180 °C, where $^{15}NO$ is no longer observed among the products, compares well with that calculated in the case of statistical coupling of N-adspecies formed via dissociation of gaseous $^{15}NO$ and gaseous $^{14}NH_3$ according to the stoichiometry:

$$6\ ^{15}NO + 4\ ^{14}NH_3 \rightarrow 5\left(^{14}N_2 + ^{15}N_2 + ^{14}N^{15}N\right) + 6\ H_2O \quad (17)$$

as shown in Table 2.

The reduction of labeled nitrates with unlabeled ammonia has also been investigated, and results are shown in Fig. 10, panel C. The reaction is detected from slightly above 150 °C, is fully selective to $N_2$ with an isotopic distribution that does not change with temperature. Note that NO has never been detected among the products. The

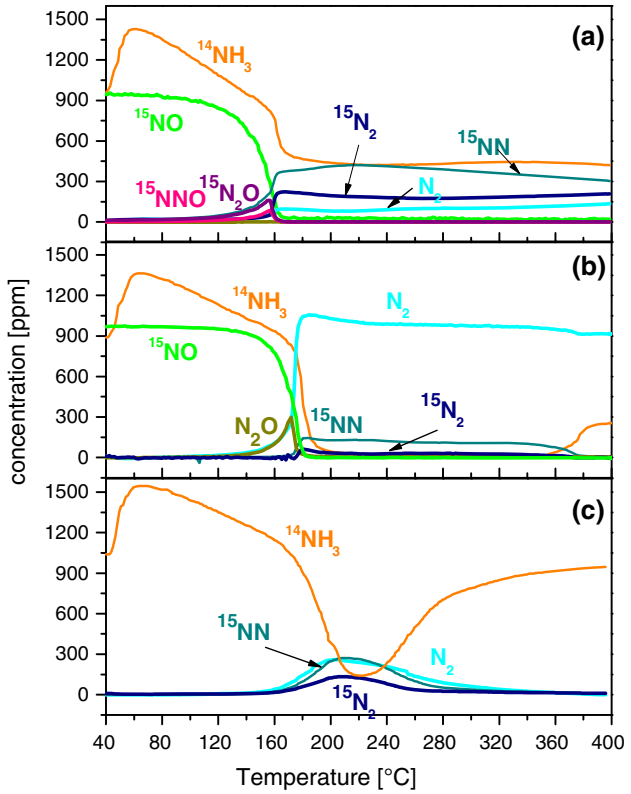


**Fig. 10** **a** TPR $^{14}NH_3$ (1,000 ppm) + $^{15}NO$ (1,000 ppm); **b** TPSR run with $^{14}NH_3$ (1,000 ppm) + $^{14}NO$ (1,000 ppm) after $^{15}NO_x$ adsorption at 350 °C (1,000 ppm $^{15}NO + O_2$ 3 % v/v in He); **c** TPSR run with $^{14}NH_3$ (1,000 ppm) after $^{15}NO_x$ adsorption at 350 °C (1,000 ppm $^{15}NO + O_2$ 3 % v/v in He)

**Table 2** Isotopic distribution of $N_2$: i) expected in case of statistical coupling of Pt-$^{15}N$ and Pt-$^{14}N$ for the reaction 6 $^{15}NO + 4\ ^{14}NH_3 \rightarrow 5\ (^{14}N_2 + {}^{15}N_2 + {}^{14}N^{15}N) + 6\ H_2O$; ii) measured during $NH_3$-TPR experiments

| Experiment/coupling mechanism | $^{14}N_2$ (%) | $^{14}N^{15}N$ (%) | $^{15}N_2$ (%) |
|---|---|---|---|
| Statistical coupling of $^{14}N$-Pt and $^{15}N$-Pt (expected) | 16 | 48 | 36 |
| (1,000 ppm $^{14}NH_3$ + 1,000 ppm $^{15}NO$)-TPR (measured) | 14 | 57 | 29 |
| (660 ppm $^{14}NH_3$ + 1,000 ppm $^{15}NO$)-TPR (measured) | 17 | 52 | 31 |

Pt-$^{14}N$ species originated from $^{14}NH_3$ and the Pt-$^{15}N$ species produced from labelled nitrates participate in the reaction in a ratio 10/6 in line with the stoichiometry constraint provided by the reaction:

$$3\ Ba(^{15}NO_3)_2 + 10\ ^{14}NH_3 \rightarrow 8(^{14}N_2 + {}^{15}N_2 + {}^{14}N^{15}N) + 3\ BaO + 15\ H_2O \quad (18)$$

leading to the following abundance of $N_2$ isotopes, calculated assuming the statistical coupling of Pt-$^{14}N$ and Pt-$^{15}N$ species: $^{14}N_2 = 39$ %, $^{14}N^{15}N = 47$ % and $^{15}N_2 = 14$ %. These numbers compare reasonably well with those measured during the $^{14}NH_3$-TPSR shown in Fig. 10, panel C and also with $^{14}NH_3$-ICSC experiments of stored labelled nitrates (Table 3). It is concluded that in the reduction of stored nitrates by ammonia, $N_2$ is produced primarily by statistical coupling of adsorbed N-atoms coming from stored $NO_x$ and gaseous $NH_3$.

**Table 3** Isotopic distribution of $N_2$: (i) expected in case of statistical coupling of Pt-$^{15}N$ and Pt-$^{14}N$ for the reaction 3 $Ba(^{15}NO_3)_2 + 10\ ^{14}NH_3 \rightarrow 8\ (^{14}N_2 + {}^{15}N_2 + {}^{14}N^{15}N) + 3\ BaO + 15\ H_2O$; (ii) measured during $NH_3$-ICSC of stored nitrates at 200 °C and at 350 °C, and during $NH_3$-TPSR of stored nitrates

| Experiment/coupling mechanism | $^{14}N_2$ (%) | $^{14}N^{15}N$ (%) | $^{15}N_2$ (%) |
|---|---|---|---|
| Statistical coupling of $^{14}N$-Pt and $^{15}N$-Pt (expected) | 39 | 47 | 14 |
| $NH_3$-ICSC at 200 °C (measured) | 45 | 43 | 12 |
| $NH_3$-ICSC at 350 °C (measured) | 50 | 35 | 15 |
| $NH_3$-TPSR (measured) | 44 | 37 | 19 |

The reaction of $^{14}NH_3$ with $^{15}NO$ (TPR experiment, Fig. 10 panel A) is faster than the reaction of $^{14}NH_3$ with the stored labelled nitrates (TPSR experiment, Fig. 10 panel C). In fact, the onset of the reaction was observed at lower temperatures in the former case (near 100 vs. near 150 °C) and the reaction proceeds till the full consumption of the limiting reactant gaseous $^{14}NO$ [77]. Besides when both gaseous NO and stored nitrates are present (Fig. 10 panel B) the reaction involving gaseous species prevails [77]. Indeed, when gaseous $^{14}NO$ is present unlabelled $N_2O$ and unlabelled $N_2$ are formed, and when gaseous $^{14}NO$ has been depleted, $^{14}NH_3$ reacts with stored labelled nitrates to give $^{14}N^{15}N$ and $^{15}N_2$ although unlabelled $N_2$ is by far the most abundant isotope. The reactivity of $NH_3$ with gaseous $^{14}NO$ seems to be slightly inhibited in the presence of stored nitrates. In fact, the onset of the $NH_3$ + NO reaction is seen at higher temperature in the presence of stored nitrates (near 120 vs. near 100 °C). Based on these results it is concluded that gaseous NO is more reactive towards $NH_3$ than stored nitrates and that the activation of the stored species represents the rate determining step in the reduction of stored nitrates. Besides, when NO is not present in the gas phase, the Pt sites are cleaned by the reducing agent and accordingly reducing conditions prevail. The primary route in the formation of di-nitrogen is the statistical coupling between N-adspecies formed upon release of $^{15}NO$ from stored nitrates and upon decomposition of $^{14}NH_3$.

The reduction of labelled nitrites stored from $^{15}NO/O_2$ at 150 °C on Pt–Ba/$Al_2O_3$ with unlabelled ammonia was also investigated [79]. Under temperature programming, the reaction is seen near 120 °C. At low T (T < 160 °C) single labelled $^{15}N^{14}N$ represents the main product (with minor

amounts of $^{15}N^{14}NO$). Then, also the other di-nitrogen isotopes are detected. The reaction was also accomplished under isothermal conditions at 150 °C by applying a step change in the concentration of $^{15}NO$ in the feed. Again single labelled $^{15}N^{14}N$ represents the main product initially (with minor amounts of $^{15}N^{14}NO$). Then also the other $N_2$ isotopes are detected. In both cases NO was never detected among the products.

The abundance of single labelled nitrogen $^{15}N^{14}N$ obtained during TPR of $^{15}NO + {}^{14}NH_3$, TPSR of stored labelled nitrite with unlabelled $NH_3$ and isothermal concentration step change experiments for the reduction of stored labelled nitrites by unlabelled $NH_3$ at low T (150 °C) is shown in Fig. 11a–c, respectively. It appears that the abundance of single labelled nitrogen $^{15}N^{14}N$ is significantly higher than that expected in the case of statistical coupling of N-ad-atoms formed from decomposition of gaseous $^{14}NH_3$ and decomposition of gaseous $^{15}NO$ or from release of stored nitrite and its further reduction (around 50 % to the best) either at low temperature (TPR and TPSR experiments) and at short time on stream (ICSC experiment at 150 °C).

Accordingly, the statistical coupling of N ad-species cannot be considered here as the unique route responsible for the formation of $N_2$. Another pathway involving the preferential coupling of NO- and $NH_3$-related species must be invoked to explain concentrations of single labeled $^{15}N^{14}N$ species significantly higher than 50 % (Fig. 12; [79]). It is worth noting that this pathway is also accompanied by the formation of $N_2O$, i.e. an oxidized N-containing species whose presence suggests that the coupling between NO- and $NH_3$-related species operates under slightly oxidizing conditions. Indeed, the presence of PtO sites prevents the NO dissociation.

Isotopic labelled experiments also provide information on the pathways involved in the formation of $N_2O$ [77–79]. As shown in Fig. 12, this species is formed in limited amounts during the reduction of stored nitrites by $NH_3$ (panel A) while amounts higher by one order of magnitude have been observed during the reaction of $^{15}NO$ (1,000 ppm) present in the feed gas with $^{14}NH_3$ (panel B). Since unlabelled $N_2O$ was not observed, $^{15}NO$ must be directly involved in the formation of $N_2O$. Accordingly and in line with literature proposals [80, 81] it was suggested that $N_2O$ formation involves either the coupling of two adsorbed NO molecule [reaction (19)] or the recombination of an adsorbed NO molecule with an adsorbed $NH_x$ fragment originated from $NH_3$ adsorption [reaction (20)]:

$$2\,{}^{15}NO_{(a)} \rightarrow {}^{15}N^{2}O_{(g)} + O_{(a)} + s \quad (19)$$

$${}^{14}NH_{x(a)} + {}^{15}NO_{(a)} \rightarrow {}^{14}N^{15}NO_{(g)} + x\,H_{(a)} \quad (20)$$

The formation of $N_2O$ is strongly affected by temperature. Indeed above 180 °C the $N_2O$ concentration is always

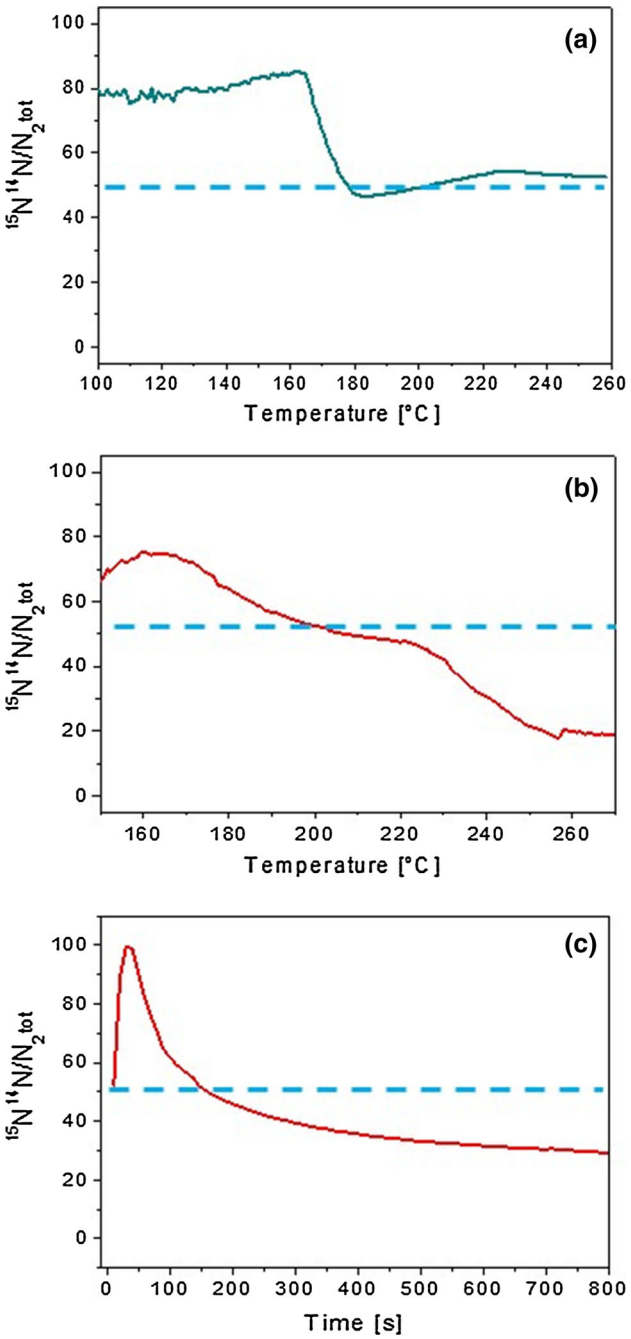


**Fig. 11** $^{15}N^{14}N$ relative abundance during **a** TPR $^{14}NH_3$ (660 ppm) + $^{15}NO$ (1,000 ppm); **b** TPSR run with $^{14}NH_3$ (1,000 ppm) after $^{15}NO_x$ adsorption at 150 °C (1,000 ppm $^{15}NO + O_2$ 3 % v/v in He); **c** ICSC run with $^{14}NH_3$ (1,000 ppm) after $^{15}NO_x$ adsorption at 150 °C (1,000 ppm $^{15}NO + O_2$ 3 % v/v in He)

negligible in the absence of oxygen. It was suggested that at high temperature NO dissociation was favored because Pt is kept in a reduced state by ammonia, so that $N_2O$ formation is prevented due to the lack of adsorbed NO species. Besides $N_2O$ could decompose onto reduced Pt sites to give $N_2$ and PtO [82].

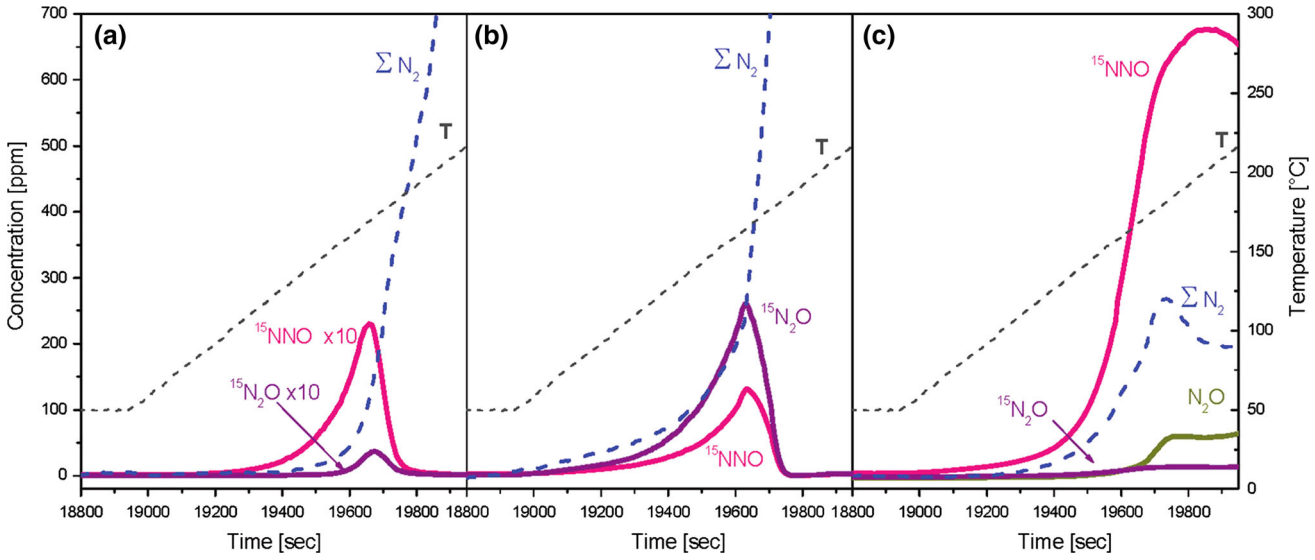


**Fig. 12** **a** TPSR run with $^{14}NH_3$ (1,000 ppm) after $^{15}NO_x$ adsorption at 150 °C (1,000 ppm $^{15}NO + O_2$ 3 % v/v in He), **b** TPR run with $^{14}NH_3$ (660 ppm) and $^{15}NO$ (1,000 ppm) in He, **c** TPR run with $^{14}NH_3$ (660 ppm), $^{15}NO$ (1,000 ppm), and $O_2$ (3 % v/v) in He over Pt–Ba/$Al_2O_3$ catalyst. (reprinted with permission from [79])

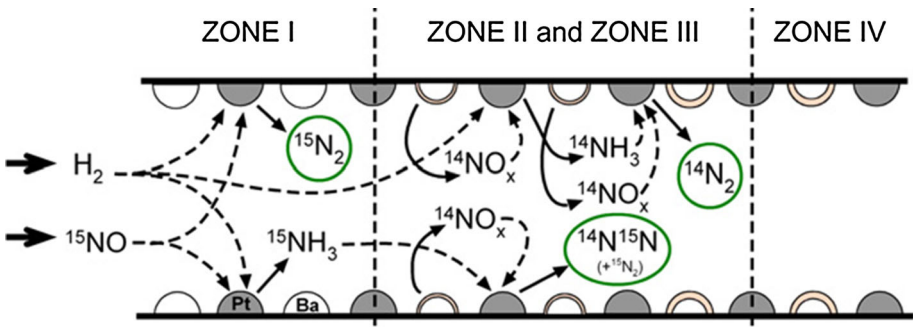


**Fig. 13** Schematic of the proposed regeneration mechanism of the LNT with hydrogen. Storage was achieved with $^{14}NO$ and regeneration was accomplished with $H_2$ in the presence of $^{15}NO$ (reprinted with permission from [82])

In the presence of oxygen (3 % v/v) in the feed stream, the nitrous oxide concentration is greater (Fig. 12, panel C) because NO dissociation is prevented over the oxygen covered Pt surface and this increases the concentration of NO adspecies. The presence of oxygen in the feed changes the nitrous oxide distribution during the TPR of $^{14}NH_3 + {}^{15}NO$: in the absence of oxygen $^{15}N_2O$ prevails over $^{14}N^{15}NO$ while in the presence of oxygen the concentration of the double-labelled nitrous oxide is negligible while that of single-labelled nitrous oxide is significantly greater. Indeed adsorbed oxygen drives reaction (19) from right to left, while it was reported to favour ammonia activation yielding reactive $NH_x$ adsorbed intermediates [83]; this eventually explains the formation in greater amounts of $^{14}N^{15}NO$.

As previously discussed, the presence of NO in the gas phase during the regeneration period could modify the reaction network for $NO_x$ reduction to $N_2$. To study the behaviour of a Pt–BaO/$Al_2O_3$ catalyst during $NO_x$ reduction when NO is also fed together with $H_2$ in the regeneration period, Pereda-Ayo et al. [82] employed isotopically labelled techniques, storing $^{14}N$ unlabelled nitrates that were reduced during the subsequent rich period, feeding labelled $^{15}NO$ together with $H_2$. All $N_2$ isotopes were detected, namely $^{15}N_2$, $^{15}N^{14}N$ and $^{14}N_2$. Three different routes for $N_2$ formation were deduced (as illustrated in Fig. 13): (i) in route 1, the incoming hydrogen reacts with stored nitrates to form $^{14}NH_3$ which further reacts with nitrates stored downstream to form $^{14}N_2$; (ii) in route 2 the incoming $^{15}NO$ reacts with hydrogen to form $^{15}NH_3$ upstream of the hydrogen front, it travels through the catalyst bed and reaches the regeneration front where it gets involved in the reduction of stored nitrates to form $^{15}N^{14}N$; (iii) in route 3 incoming $^{15}NO$ reacts with hydrogen to form $^{15}N_2$.

## 4 Combined Systems: LNT + SCR and DPNR

### 4.1 LNT + SCR

It has been shown that $NH_3$ is formed during regeneration of LNT catalysts, while it is well known that SCR catalysts

store large quantities of $NH_3$ under reaction conditions [84]. Hence, combining the LNT catalyst with a downstream SCR catalyst offers a potential of capturing $NH_3$ generated over the LNT and using it to convert $NO_x$ that slips through the LNT [85]. These LNT + SCR coupled systems result in higher $NO_x$ removal and lower $NH_3$ slip compared to the LNT-only systems. The LNT + SCR concept has been commercially demonstrated on the Mercedes E320 Bluetec vehicle [13] which utilized relatively high-loaded PGM LNT in combination with an Fe-based zeolite SCR catalyst. This approach is variously referred to as an in situ, hybrid, booster, or passive LNT + SCR system.

Most of the fundamental studies have involved model catalysts tested in simple laboratory gas mixtures and with hydrogen as the reducing agent. For example, Corbos et al. [86, 87] showed that the $NO_x$ removal efficiency can be greatly improved under lean–rich atmosphere if a NSR catalyst is physically mixed with Cu-ZSM-5. Indeed, Fig. 14 shows the $NO_x$ removal efficiency during the lean–rich cycles for the different catalyst mixtures (Pt–RhBa and SCR catalysts). The $NO_x$ removal activity of Pt–RhBa catalyst shows a volcano type curve and reaches a maximum of 50 % at 300 °C. Figure 14 points out that mixing the Pt–RhBa catalyst with AgAl catalyst has no significant influence on the $NO_x$ removal activity as compared to mixing with bare $\alpha$-$Al_2O_3$, regardless of temperature. On the other hand, the $NO_x$ removal activity was improved in 200–300 °C temperature range by mixing Pt–RhBa catalyst with CoAl or CuZSM-5. A remarkable difference is observed at 250 and 300 °C. At these temperatures, the activity of Pt–RhBa + CuZSM-5 mixed catalyst is much higher than that obtained with Pt–RhBa + CoAl [85, 86, 88].

In most of these studies, NSR experiments have been performed by alternating long lean phases with short rich periods characterized by high concentration of the reductant. Accordingly, significant temperature effects may have occurred. In view of this, only a qualitative analysis of the data has been generally attempted.

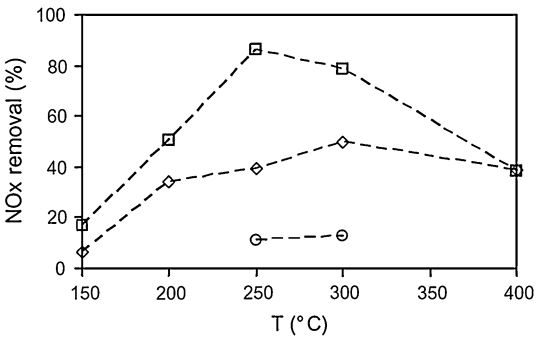


**Fig. 14** $NO_x$ removal efficiency (%) during the lean–rich cycles for physically mixed catalysts (*diamond*) Pt–RhBa + $\alpha$-$Al_2O_3$, (*cross symbol*) Pt–RhBa + AgAl, (*square*) Pt–RhBa + CuZSM-5 and (*triangle*) Pt–RhBa + CoAl. Reaction conditions: lean 100 s, 1 % $CO_2$, 500 ppm NO, 10 % $O_2$, 0.13 % $CO/H_2$ (75/25), 167 ppm $C_3H_6$ and rich 10 s with 8.53 % $CO/H_2$ (75/25), 100 ppm NO, 1 % $CO_2$ (reprinted with permission from [86])

A systematic investigation of the hybrid arrangements LNT + SCR has also been accomplished in our labs [89, 90], which combines reactivity measurements performed under nearly isothermal conditions (i.e. with low concentration of NO and of the reductant) and in situ FT-IR spectroscopy to analyse the species formed in the gas phase and at the catalyst surface during the lean–rich cycles, covering the temperature range 150–350 °C and also considering the presence of $H_2O$ and $CO_2$ in the exhausts. Pt–Ba/$Al_2O_3$ LNT catalyst and Fe-ZSM-5 SCR catalyst have been tested alone in a typical NSR adsorption-reduction cycle. Then both LNT + SCR dual bed and LNT/SCR physical mixture have been tested in the same conditions. $NO_x$ removal efficiency, $N_2$ production during the lean and rich periods, $NH_3$ oxidation upon $O_2$ admission during the lean phase and $NH_3$ slip were determined and explained at the quantitative level for all the mentioned arrangements and the results obtained during lean–rich experiments performed at 250 °C are reported in Table 4. From this quantitative analysis, and the FT-IR evidences, it has been possible to provide a picture of the working mechanism of these combined catalytic systems, depicted in Fig. 15. During the lean phase, the storage of $NO_x$ ($NO_x$ stored in Table 4) occurs primarily on Pt–Ba/$Al_2O_3$ and results in the formation of nitrate species, well recognized by FTIR at the end of the lean phase (bands at 1,416, 1,328 and 1,035 $cm^{-1}$). Moreover, the FT-IR study showed that the Fe-ZSM-5 SCR catalyst is able to adsorb large amounts of ammonia, the trapping of $NH_3$ being most favoured at low temperatures. Accordingly, during the rich phase of a NSR cycle the ammonia produced in the stored $NO_x$ reduction can be adsorbed by Fe-ZSM-5 SCR catalyst of the combined LNT + SCR catalytic system (both physical mixture or dual bed).

As it clearly appears from the sketch of Fig. 15, and the data of Table 4, the $NO_x$ removal efficiency ($NO_x$ removed in Table 4) is always higher for both hybrid LNT + SCR systems due to the contribution of $N_2$ produced by the SCR reactions over the Fe-ZSM-5 catalyst during the lean phase ($N_2$ lean) in addition to $NO_x$ stored onto the LNT catalyst during the lean phase ($NO_x$ stored in Table 4). For all investigated systems (LNT, LNT + SCR physical mixture and LNT + SCR dual bed) the amounts of $NO_x$ removed correspond to amounts of $NO_x$ stored plus those of $N_2$ lean.

The ammonia species adsorbed during the rich phase are completely consumed by the SCR reactions upon subsequent admission of $NO/O_2$ to produce $N_2$ ($N_2$ lean in Table 4). Until the ammonia is present on the surface of the SCR catalyst, the only observable $NO_x$ surface species are $Fe^{3+}$(NO) indicating that NO is directly bonded at Fe sites

**Table 4** Results of lean–rich experiments performed over LNT (Pt–Ba/$Al_2O_3$), LNT + SCR (Fe-ZSM-5) physical mixture and LNT/SCR dual bed arrangements

| Amounts ($10^{-6}$ mol/$g_{cat}$) | LNT | LNT + SCR (phys. mix.) | LNT + SCR (dual bed) |
|---|---|---|---|
| In absence of $CO_2$ and $H_2O$ | | | |
| $NO_x$ removed, lean phase | 429 | 512 | 472 |
| $NO_x^{removed,leanphase} = NO_x^{fed} - NO_x^{out}$ | | | |
| $N_2$ lean | 0 | 78 | 49 |
| $NO_x$ stored, lean phase | 429 | 434 | 423 |
| $NO_x^{stored,leanphase} = NO_x^{removed,leanphase} - N_2^{leanphase}$ | | | |
| $N_2$ rich | 193 | 51 | 209 |
| $N_2 + N_2O + NO_x$ at $O_2$ admission | 0 | 142 | 0 |
| Moles of N-containing species formed upon $O_2$ admission | | | |
| $NH_3$ slip | 57 | 70 | 14 |

Experimental conditions: catalyst weight: 60 mg LNT or 60 mg LNT + 60 mg SCR; T = 250 °C; total flow rate 100 $Ncm^3$/min; lean phase: NO (1,000 ppm) in 3 % $O_2$ + He; rich phase: $H_2$ (2,000 ppm) in He; absence of $CO_2$ and $H_2O$ or $CO_2$ = 0.1 % (v/v) and $H_2O$ = 1 % (v/v)

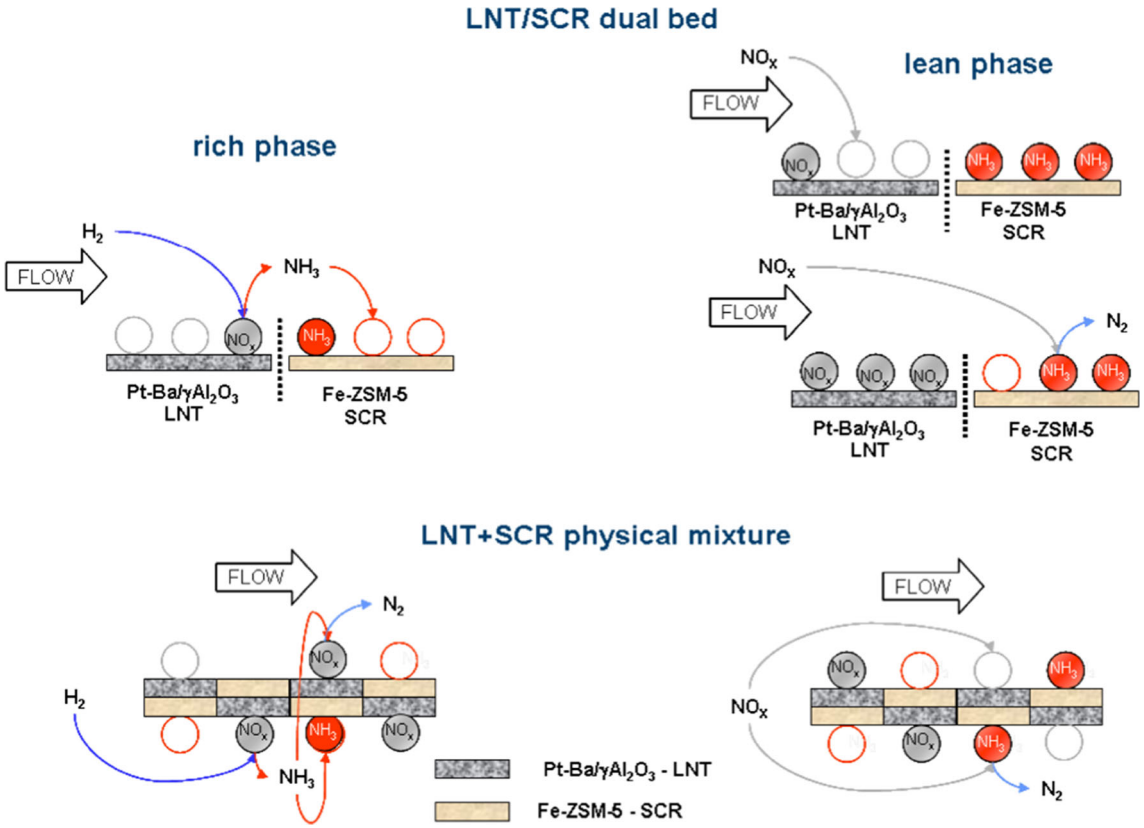


**Fig. 15** Sketch of the behavior of hybrid LNT-SCR catalytic systems, physical mixture and dual bed

(band at 1,878 $cm^{-1}$). After adsorbed ammonia is completely consumed, the increase of $NO^+$ (peak at 2,132 $cm^{-1}$) and nitrate (main peaks at 1,628 $cm^{-1}$ and at 1,573 $cm^{-1}$) species is observed together with the erosion of the band related to $Fe^{3+}$(NO) species. This indicates that at first SCR reaction takes place and then small amounts of $NO_x$ are stored at the catalyst surface as nitrates [91].

When the hybrid LNT + SCR systems are considered, in the reduction of nitrates stored over Pt–Ba/$Al_2O_3$, $N_2$ is formed during the rich phase ($N_2$ rich in Table 4) together with $NH_3$, that is trapped onto the Fe-ZSM-5 catalyst in the form of coordinated $NH_3$ (absorptions in the region 3,500–3,100 $cm^{-1}$ and at 1,616 $cm^{-1}$) and of protonated $NH_4^+$ (absorptions in the region 3,000–2,250 $cm^{-1}$ and at 1,447 $cm^{-1}$).

In the NSR cycle, $NH_3$ trapped onto Fe-ZSM-5 during the rich phase is oxidized during the subsequent lean phase immediately after $O_2$ admission to give $N_2$, $N_2O$, and $NO_x$ ($N_2 + N_2O + NO_x$ at $O_2$ admission in Table 4) and upon subsequent NO admission to give $N_2$ according to standard and fast SCR reactions ($N_2$ lean). Therefore, the amount of $NH_3$ stored during the rich phase over the Fe-ZSM-5 particles is obtained by the sum of amounts of $N_2 + N_2O + NO_x$ at $O_2$ admission and of amounts of $N_2$ lean; this sum is always higher for the physical mixture than for the dual bed. It turns out that the trapping of $NH_3$ is most favoured when the particles of Pt–Ba/$Al_2O_3$ and of Fe-ZSM-5 are evenly distributed in the catalyst bed, as in the case of the LNT + SCR physical mixture. Trapping the $NH_3$ onto the Fe-ZSM-5 particles prevents the reaction of $NH_3$ with $NO_x$ stored downstream onto Pt–Ba/$Al_2O_3$ particles to give $N_2$ during the rich phase ($N_2$ rich in Table 4), that in fact is lower for the physical mixture than for the dual bed.

It is worth noting that the oxidation of $NH_3$ trapped onto the Fe-ZSM-5 particles after admission of $O_2$ was observed only in the case of the physical mixture and was ascribed to desorption of ammonia from the Fe-ZSM-5 particles followed by reaction over the Pt–Ba/$Al_2O_3$ in close proximity. The selectivity to nitrogen for this reaction increases significantly with temperature and is almost complete at 350 °C. The adsorption of $NH_3$ over the zeolite catalyst during the rich phase and its consumption during the subsequent lean phase is documented by the FT-IR study. No other intermediate species have been detected.

In conclusion, due to the fact that ammonia, formed in the reduction of nitrates by hydrogen over the LNT catalyst, can be effectively stored onto the SCR catalyst, the $NO_x$ removal efficiency is increased and the ammonia slip is reduced over the coupled LNT + SCR systems. The ammonia slip is reduced to the best over the dual bed arrangement (LNT ahead of SCR). The synergy becomes more important with the aged NSR catalyst where generally higher $NH_3$ yields are observed in comparison with the fresh NSR catalyst [91].

The class of combined LNT + SCR catalysts also comprises the system developed by Sato and coworkers [92] consisting of a solid acid SCR catalyst and Pt/OSC (oxygen storage component) such as $CeO_2/ZrO_2$ as NSR catalyst.

### 4.2 DPNR

The DPNR (Diesel Particulate-$NO_x$ Reduction) technology aimed at the simultaneous reduction of PM and $NO_x$ was developed by Toyota [16, 93]. The catalytic converter for DPNR is a porous ceramic wall-flow filter coated with a NSR catalyst. Like the NSR technology, this system accomplishes the removal $NO_x$ under cyclic lean/rich conditions; in addition the simultaneous soot abatement occurs, mainly under lean conditions due to the presence of $NO_x$ and the excess oxygen in the exhaust gas. Of note, Toyota researchers also proposed that active oxygen species, which are formed during $NO_x$ adsorption, are effective in soot oxidation under rich conditions as well.

Castoldi et al. [94] showed that under cycling conditions, i.e. alternating lean/rich phases, the Pt–Ba/$Al_2O_3$ NSR system is able to simultaneously remove $NO_x$ and soot.

Soot combustion was primarily ascribed to the $NO_2$ formed upon NO oxidation over Pt, and to the occurrence of the NO recycling to $NO_2$ [95]. Moreover, based on a comparative study of Pt–Ba/$Al_2O_3$ and Pt/$Al_2O_3$, a role of the stored $NO_x$ in the oxidation of soot has been suggested [96], which is in agreement with the results of Suzuki and Matsumoto [16] who noted a higher combustion activity of soot when a $NO_x$ trap material is incorporated in the catalyst. Actually, there is a general consensus on the fact that the $NO_x$ storage function of the LNT catalysts positively affects the combustion of soot by providing an additional path for oxidation of the carbonaceous material in addition to the well-established gas-phase reactions involving $O_2$ and $NO_2$. Kustov et al. [97] reported that the stored nitrates may decrease the onset temperature of soot oxidation when nitrate decomposition occurs in a proper temperature range, due to the release of $NO_2$ in the gas phase. Along similar lines, Sullivan et al. [98] reported that the presence of a $NO_x$ trapping component like BaO in Pt/$SiO_2$ systems does not promote per se the particulate combustion, but favors soot combustion due to the increase in the $NO_2$ gas phase concentration, observed upon nitrates decomposition during LNT catalyst regeneration.

However more recently, some of us investigated the reactivity of stored nitrates during TPD (temperature programmed desorption)/TPO (temperature programmed oxidation) experiments carried out over Ba- and K-based LNT systems and suggested that stored nitrates take a direct part in soot oxidation, which indeed is observed below the temperature threshold for nitrates thermal decomposition [96, 99, 100]. In particular a redox mechanism occurring between nitrates, acting as oxidant agents toward soot, and soot particles, acting as reducing centres, has been suggested. This hypothesis is in agreement with the results obtained by Ito et al. [101] over Cs-$MnO_x$–$CeO_2$ catalysts and by Sanchez et al. [102, 103] over lanthanum supported catalysts containing noble metals.

Several authors reported that the activity of LNT catalysts for soot combustion is higher in the presence of K rather than of Ba [104–106]. A direct role of the alkali or alkaline-earth component in the oxidation of soot has been pointed out, which seems to be superimposed to the gas

phase soot combustion activity by $NO_2$. It has been suggested [107, 108] that potassium may favor the soot oxidation through the formation of low melting point compounds, thus improving the mobility of the active surface species and favoring the contact between the soot and the catalyst which has been claimed to be a key factor in the oxidation of soot [109]. More recently, Castoldi et al. [110] investigated the intrinsic reactivity of alkaline (Na, K, Cs)—and alkaline/earth (Ca, Ba, Mg)—based catalysts in the oxidation of soot, and prepared samples in which the active elements were deposited directly onto the soot particles (''full contact'' conditions). The reactivity in the soot combustion of the selected elements has been correlated with their electronegativity, with the overall activity ranking ($Cs \geq K > Ba > Na > Ca \gg Mg$) which follows the electropositivity order of the investigated elements. Notably, under these conditions, the performance of the poorly reactive Ba-containing sample became more comparable to that of the very active K-based system.

It is worth noting that, when considering the loose contact systems the correlation between electropositivity and activity in the soot combustion is not more apparent. This indicates that under these conditions other parameters play a major role in the activity, thus confirming that the high activity of K-based systems, even under loose conditions, is likely due to the high mobility of the K surface species. It has been noted that NSR catalysts can suffer for the loss of the alkali or alkaline-earth metal oxide in view of its surface mobility. Indeed Krishna and Makkee [104] found Pt-$K/Al_2O_3$ catalyst to be more active but less stable than Pt–$Ba/Al_2O_3$.

Finally, several studies have pointed out the negative effect of soot on the $NO_x$ storage behavior of the LNT catalysts [99, 100, 105, 106]. Sullivan et al. [111] showed that the presence of soot decreases the $NO_x$ storage capacity of a Pt–$Ba/SiO_2$ system at 400 °C; in particular they hypothesized that soot may compete with Ba sites for reaction with $NO_2$ by offering another reaction path for the utilization of $NO_2$ rather than the desired formation of surface nitrates. Along similar lines, Artioli et al. [99] observed that soot decreases the $NO_x$ storage capacity of Pt–$Ba/Al_2O_3$ system and favors the decomposition and reduction of the stored nitrates, while soot is being oxidized. A direct reaction between the stored nitrates and soot was suggested, that has been explained with the surface mobility of the adsorbed nitrates. More recently Klein et al. [112, 113] attributed the decrease in the $NO_x$ storage capacity of Pt–$Ba/Al_2O_3$ catalysts to the destabilization of stored nitrates via a direct surface reaction with carbon particles.

In conclusion, very few investigations deal with the effect of soot on the regeneration of LNT catalysts. Nakatani et al. [93] observed that the $NO_x$ conversion efficiency of DPNR catalysts is almost similar to that of the soot-free NSR catalysts. This is confirmed by investigations performed within our group [96, 99, 100].

## 5 Perspectives

The development of successful catalytic technologies for the control of $NO_x$ emissions from vehicles under lean conditions over the last 20 years has been a remarkable technical achievement. Catalytic lean $NO_x$ removal converters are of commercial importance and extensive research has been done on several aspects of their formulation, synthesis and performance. Presently SCR and NSR represent the top contenders for lean $NO_x$ removal. SCR is a more mature technology that requires an on board urea tank so that it is used mostly for HD and high segment vehicles but it is considered as well for LD vehicles and passenger cars. NSR does not require big layout modification because it uses the exhaust as the reducing agent and is the favored approach for low segment vehicles.

In spite of the fact that the purpose of this paper was not to compare one technology with the other, but to address the reaction process fundamentals of the NSR technology, still a comparison between NSR and SCR technologies is worthwhile in order to enlighten analogies and differences in the associated chemistries and catalyst functionalities.

History teaches us that the advances in technology will come mostly from the application and that fundamental insight of such advances usually comes later. Experimental and theoretical tools are now available that allow us to better understand the details of the catalytic chemistry of NSR. Among these special importance has been (and it is expected that more will be in the future) the use of spatially resolved analytical tools such as capillary inlet mass spectrometry (SpaciMS) to provide a spatiotemporal resolution during transient storage and regeneration processes occurring over NSR catalysts, of isotopic experiments to address the mechanism of $NO_x$ release and of $N_2$ formation and of spectro- kinetics to combine the analysis of gas phase and surface concentrations.

It is noted that coupled LNT + SCR systems, that use the LNT to generate ammonia during the rich period of the cycle and then store and use ammonia in a downstream SCR catalyst, are of special interest nowadays. They are being optimized to ensure high $NO_x$ removal efficiencies while reducing the PGM usage and are moving onto much more vehicle testing. Ammonia generation from the NSR and finding optimum system configurations are at the forefront [12].

Recently a very interesting phenomenon that achieves high $NO_x$ conversion was observed over NSR catalysts by Toyota researchers [114]. This phenomenon occurs when

continuous short cycle injections of hydrocarbons are supplied at a predetermined concentration in lean conditions. The system that uses this concept was named Di-Air (diesel $NO_x$ after-treatment by adsorbed intermediate reductant) because it was concluded that such a phenomenon is likely due to the generation of reactive intermediates formed by adsorbed $NO_x$ over the base catalysts and HCs partially oxidized. It is recommended that the Di-Air concept should be studied more deeply by the scientific community.

Besides, the nitrite route, which was found to dominate at low temperatures during the storage of $NO/O_2$ over LNT catalysts, suggests we should revisit the chemistry of NO oxidation to $NO_2$ since in this case the reaction proceeds through a stepwise oxidation to form nitrites that are stabilized against further reaction to form $NO_2$ by the interaction with nearby Ba sites.

Finally, it has been shown that nitrites and nitrates stored species exhibit different stability and reactivity during the reduction process. These aspects could be investigated in details and the possible implications and/or challenges explored.

**Acknowledgments** The authors thank Dr. William Epling for useful discussion and suggestions.

## References

1. http://delphi.com/manufacturers/auto/powertrain/emissions_standards/. Accessed 18 Aug 2014
2. Johnson T (2008) Platin Met Rev 52(1):23
3. Twigg MV (2013) Platin Met Rev 57(3):192
4. Forzatti P (2001) Appl Catal A 222:221
5. Kato A, Matsuda S, Kamo T, Nakajima F, Kuroda H, Narita T (1981) J Phys Chem 85:4099
6. Koebel M, Elsener M, Madia G (2001) Ind Eng Chem Res 40:52
7. Takahashi N, Shinjoh H, Iijima T, Suzuki T, Yamazaki K, Yokota K, Suzuki H, Miyoshi M, Matsumoto S, Tanizawa T, Tanaka T, Tateishi S, Kasahara K (1996) Catal Today 27:63
8. Matsumoto S (2000) CATTECH 4:102
9. Epling WS, Campbell IE, Yezerets A, Currier NW, Park JE (2004) Catal Rev Sci Eng 46:163
10. Engstrom P, Ambernstsson A, Skoglundh M, Fridell F, Smedler G (1999) Appl Catal B 22:241
11. Sedlmair C, Seshan K, Jentys A, Lercher JA (2002) Catal Today 75:413
12. Johnson T (2010) Platin Met Rev 54:216
13. Weibel M, Waldbüβer N, Wunsch R, Chatterjee D, Bandi-Konrad B, Krutzsch B (2009) Top Catal 52:1702
14. Jelles SJ, Makkee M, Moulijn JA (2001) Top Catal 16:269
15. Setiabudi A, Makkee M, Moulijn JA (2004) Appl Catal B 50:185
16. Suzuki J, Matsumoto S (2004) Top Catal 28:171
17. Fridell E, Persson H, Westerberg B, Olsson L, Skoglundh M (2000) Catal Lett 66:71
18. Mahzoul H, Brilhac JF, Gilot P (1999) Appl Catal B 20:47
19. Prinetto F, Ghiotti G, Nova I, Lietti L, Tronconi E, Forzatti P (2001) J Phys Chem B 105:12732
20. Lietti L, Daturi M, Blasin-Aubé V, Ghiotti G, Prinetto F, Forzatti P (2012) Chem Cat Chem 4:55
21. Westerberg B, Fridell E (2001) J Mol Catal A 165:249
22. Schmitz P, Baird R (2002) J Phys Chem B 106:4172
23. Prinetto F, Ghiotti G, Nova I, Castoldi L, Lietti L, Forzatti P (2003) Phys Chem Chem Phys 105:4428
24. Nova I, Castoldi L, Prinetto F, Ghiotti G, Lietti L, Tronconi E, Forzatti P (2004) J Catal 222:377
25. Visconti CG, Lietti L, Manenti F, Daturi M, Corbetta M, Pierucci S, Forzatti P (2013) Top Catal 56:311–316
26. Morandi S, Prinetto F, Ghiotti G, Castoldi L, Lietti L, Forzatti P, Daturi M, Blasin-Aubé V (2014) Catal Today 231:116–124
27. Weiss BM, Caldwell KB, Iglesia E (2011) J Phys Chem C 115:6561
28. Epling WS, Peden CHF, Szanyi J (2008) J Phys Chem C 112:10952
29. Chaugule SS, Kispersky VF, Ratts JL, Yezerets A, Currier NW, Ribeiro FH, Delgass WN (2011) Appl Catal B 107:26
30. Lietti L, Forzatti P, Nova I, Tronconi E (2001) J Catal 204:175
31. Lindholm A, Currier NW, Friedell E, Yezerets A, Olsson L (2007) Appl Catal B 75:78
32. Cant NW, Liu IOY, Patterson MJ (2006) J Catal 243:309
33. Nova I, Lietti L, Castoldi L, Tronconi E, Forzatti P (2006) J Catal 239:244
34. Castoldi L, Nova I, Lietti L, Tronconi E, Forzatti P (2004) Catal Today 96:43
35. Clayton RD, Harold MP, Balakotaiah V, Wan CZ (2009) Appl Catal B 90:662
36. Tuttlies U, Schmeisser V, Eigenberger G (2004) Chem Eng Sci 59:4731
37. Kabin KS, Muncrief RL, Harold MP (2004) Catal Today 96:79
38. Muncrief RL, Kabin KS, Harold MP (2004) AIChE J 50:2526
39. Amberntsson A, Persson H, Engström P, Kasemo B (2001) Appl Catal B 31:27
40. Liu Z, Anderson JA (2004) J Catal 224:18
41. Cant NW, Patterson MJ (2003) Catal Lett 85:153
42. Poulston S, Rajaram R (2003) Catal Today 81:603
43. Zho GU, Luo T, Gorte RJ (2006) Appl Catal B 64:88
44. Epling WS, Parks JE, Campbell GC, Yezerets A, Currier NW, Campbell LE (2004) Catal Today 96:21
45. Otto K, Shelef M, Kummer JT (1970) J Phys Chem 74:2690
46. Bathia D, Harold MP, Balakotaiah V (2010) Catal Today 151:314
47. Coronado J, Anderson J (1999) J Mol Catal A 138:83
48. Righini L, (2014) NO*x* Storage-Reduction (NSR) catalytic process for NO*x* removal from mobile sources, PhD Thesis, Politecnico di Milano
49. Clayton RD, Harold MP, Balakotaiah V (2008) Appl Catal B 84:616
50. Partridge WP, Choi JS (2009) Appl Catal B 91:144
51. Mulla SS, Chaugule SS, Yezerets A, Currier NW, Delgass WN, Ribeiro FH (2008) Catal Today 136:136
52. Cumaranatunge L, Mulla SS, Yezerets A, Currier NW, Delgass WN, Ribeiro FH (2007) J. Catal. 246:29
53. Nova I, Lietti L, Forzatti P (2008) Catal Today 136:128
54. Lietti L, Nova I, Forzatti P (2008) J Catal 257:270
55. Stoica M, Caldararu M, Ionescu NI, Auroux A (2000) Appl Surf Sci 153:218
56. Szailer T, Kwak JH, Kim DH, Hanson JC, Peden CHF, Szanyi J (2006) J Catal 239:51
57. Forzatti P, Lietti L, Gabrielli N (2010) Appl Catal B 99:145
58. Pihl JA, Parks JE, Daw CS, Root TW (2006) SAE Technical Paper 01-3441
59. Abdulhamid H, Fridell E, Skoglundh M (2006) Appl Catal B 62:319

60. Abdulhamid H, Fridell E, Skoglundh M (2004) Top Catal 30(31):161
61. Di Giulio C, Komvokis VG, Amiridis MD (2011) Catal Today 184:8
62. Forzatti P, Lietti L, Nova I, Morandi S, Prinetto F, Ghiotti G (2010) J Catal 274:163
63. Castoldi L, Lietti L, Bonzi R, Artioli N, Forzatti P, Morandi S, Ghiotti G (2011) J Phys Chem C 115:1277
64. Morandi S, Ghiotti G, Castoldi L, Lietti L, Nova I, Forzatti P (2011) Catal Today 176:399
65. Lasage T, Verrier C, Bazin P, Saussey J, Daturi M (2003) Phys Chem Chem Phys 5:4435
66. Bion N, Saussey J, Haneda M, Daturi M (2003) J Catal 217:47
67. Scholz CMI, Maes BHW, de Croon MHJM, Schoulten JC (2007) Appl Catal A 332:1
68. Ji Y, Toops TJ, Crocker M (2013) Appl Catal B 140–141:265
69. Okuhara T, Hasada Y, Misono M (1997) Catal Today 35:83
70. Kameoka S, Chafik T, Ukisu Y, Miyadera T (1998) Catal Lett 55:211
71. Ukisu Y, Miyadera T, Abe A, Yoshida K (1996) Catal Lett 39:265
72. Sumiya S, He H, Abe A, Takezawa N, Yoshida K (1998) J Chem Soc Faraday Trans 94:2217
73. Nova I, Lietti L, Forzatti P, Prinetto F, Ghiotti G (2010) Catal Today 151:330
74. Dasari P, Muncrief R, Harold M (2013) Top Catal 56:1922
75. Castoldi L, Lietti L, Righini L, Forzatti P, Morandi S, Ghiotti G (2013) Top Catal 56:193
76. van Tol MFH, Siera J, Cobden PD, Nieuwenhuys BE (1992) Surf Sci. 274(1):63
77. Lietti L, Righini L, Castoldi L, Artioli N, Forzatti P (2013) Top Catal 56:7
78. Righini L, Castoldi L, Lietti L, Da Costa P, Sauce, Forzatti P (2013) Top Catal 56:1906
79. Lietti L, Artioli N, Righini L, Castoldi L, Forzatti P (2012) Ind Eng Chem Res 51:7597
80. Burch R, Shestov AA, Sullivan JA (1999) J Catal 188:69
81. Burch R, Daniells ST, Hu P (2002) J Chem Phys 117:2092
82. Pereda-Ayo B, González-Velasco JR, Burch R, Hardacre C, Chansai S (2012) J Catal 285:177
83. Perez-Ramirez J, Kondratenko EV, Kondratenko VA, Baerbs M (2005) J Catal 229:303
84. Tronconi E, Lietti L, Forzatti P, Malloggi S (1966) Chem Eng Sci 51:2965
85. Can F, Curtois X, Royer S, Blanchard G, Rousseau S, Duprez D (2012) Catal Today 197:144
86. Corbos EC, Haneda M, Courtois X, Marecot P, Duprez D, Hamada H (2008) Catal Commun 10:137
87. Corbos EC, Haneda M, Courtois X, Marecot P, Duprez D, Hamada H (2009) Appl Catal A 365:187
88. Wang J, Ji Y, He Z, Crocker M, Dearth M, McCabe RW (2012) Appl Catal B 111(112):562
89. Forzatti P, Lietti L (2010) Catal Today 155:131
90. Castoldi L, Bonzi R, Lietti L, Forzatti P, Morandi S, Ghiotti G, Dzwigaj S (2011) J Catal 282:128
91. Chatterjee D, Koci P, Schmeiβer V, Marek M (2010) Krutzch B 151:395
92. Nakatsuji T, Matsubara M, Rouistenmaki J, Sato N, Ohno H (2007) Appl Catal B 77:190
93. Nakatani K, Hirota S, Takeshima S, Itoh K, Tanaka T (2002) SAE Technical Paper SP- 1674 01-0957
94. Castoldi L, Matarrese R, Lietti L, Forzatti P (2006) Appl Catal B 64:25
95. Setiabudi A, van Setten BAAL, Makkee M, Moulijn JA (2002) Appl Catal B 35:159
96. Matarrese R, Castoldi L, Lietti L (2012) Catal Today 197:228
97. Kustov AL, Makkee M (2009) Appl Catal B 88:263
98. Sullivan JA, Keane O, Cassidy A (2007) Appl Catal B 75:102
99. Artioli N, Matarrese R, Castoldi L, Lietti L, Forzatti P (2011) Catal Today 169:36
100. Matarrese R, Artioli N, Castoldi L, Lietti L, Forzatti P (2012) Catal Today 184:271
101. Ito K, Kishikawa K, Watajima A, Ikeue K, Machida M (2007) Catal Commun 8:2176
102. Sánchez BS, Querini CA, Miró EE (2009) Appl Catal A 366:166
103. Sánchez BS, Querini CA, Miró EE (2011) Appl Catal A 392:158
104. Krishna K, Makkee M (2006) Catal Today 114:48
105. Pieta IS, García-Diéguez M, Herrera C, Larrubia MA, Alemany LJ (2010) J Catal 270:256
106. Matarrese R, Castoldi L, Lietti L, Forzatti P (2007) Top Catal 42(43):293
107. Querini CA, Cornaglia LM, Ulla MA, Miró EE (1999) Appl Catal B 20:165
108. An H, McGinn PJ (2006) Appl Catal B 62:45
109. Neeft JPA, Makkee M, Moulijn JA (1996) Appl Catal B 8:57
110. Castoldi L, Matarrese R, Lietti L, Forzatti P (2009) Appl Catal B 90:278
111. Sullivan JA, Dulgheru P (2010) Appl Catal B 99:235
112. Klein J, Fechete I, Bresset V, Garin F, Tschamber V (2012) Catal Today 189:60
113. Klein J, Wu D, Tschamber V, Fechete I, Garin F (2013) Appl Catal B 132(133):527
114. Bisaiji Y, Yoshida K, Inoue M, Umemoto K, Fukuma T (2012) SAE Int J Fuels Lubr. 5(1):380